nature communications

Article

https://doi.org/10.1038/s41467-025-64675-6

Site-specific ligase-dependent conjugation with ring-opening linker improves safety and stability of HER2-targeting ADCs

Received: 12 June 2025

Accepted: 24 September 2025

Published online: 03 November 2025

Check for updates

Lei Huang[1,6], Gang Qin[2,3,6] ✉, Chengcheng Gong[4,6], Yajun Sun[2,3,6], Hui Yang[2,3], Cao Lv[2,3], Chong Liu[2,3], Lu Jiang[2,3], Jinduo Yuan[2,3], Mingyu Hu[2,3], Xinju Gao[2,3], Jun Yang[2,3], Xuesong Li[2,3], Yu Si[2,3], Paul Song[2,3] ✉, Yan Shi[2,3] ✉, Lili Shi[2,3] ✉, Bo Yang[5] ✉ & Biyun Wang[4] ✉

Most of current ADCs have the problems of heterogeneity and payload-mediated off-target toxicities due to random conjugation and unstable linker. Herein we apply site-specific ligase-dependent conjugation (LDC) for GQ1001 and GQ1005, where humanized anti-HER2 antibody is linked to DM1 and DXd, respectively, via stable ring-opening linker. GQ1001 exhibits HER2 expression-dependent activity (contrary to T-DM1), indicating decreased off-target toxicity. The biostability of GQ1001 and GQ1005 in plasma is more favorable, and pharmacokinetics and safety profiles are improved in cynomolgus-monkeys with decreased circulating free-toxin levels. GQ1001 and GQ1005 are effective in animal models against pretreated HER2-positive cancers insensitive to HER2-targeting and/or chemotherapeutic drugs. The efficacy of GQ1001 is supra-additively enhanced by tyrosine-kinase inhibitors or chemotherapy, with manageable toxicity. GQ1001 is efficacious in cancers resistant to T-DXd due to high ABCG2 expression. Together, the LDC technology and ring-opening linker improve the stability and safety in GQ1001 and GQ1005 for treating refractory HER2-positive cancers.

Toxicity remains a key issue in the development of antibody-drug conjugates (ADCs)[1]. A vital role of an ADC linker is to allow efficient drug release to target cells while maintaining stable antibody-drug linkage in circulation; the efficacy and toxicity of ADCs were thus directly and largely affected by linker stability[2]. At present, more than 80% of the marketed ADCs, including Aidixi® (Disitamab Vedotin, RC48), use the technology of Michael-addition conjugation between cysteine residues from reduced interchain disulfide bond and maleimide, which produces thiosuccinimide structures. While lysine residues-based conjugation is applied for Kadcyla® (trastuzumab-emtansine, T-DM1), Michael-addition reaction between sulfhydryl and maleimide still takes place in the second conjugation reaction, which also produces thiosuccinimide structure fragments (Fig. 1A). A prominent issue associated with the cysteine-maleimide- or thiol-maleimide-based conjugation is that the thiosuccinimide structure is not stable enough under physiological condition, and is prone to retro-

[1]National Key Laboratory of Immunity and Inflammation, National Clinical Research Center for Digestive Diseases, Changhai Clinical Research Unit, Department of Gastroenterology, The First Affiliated Hospital of Naval Medical University/Changhai Hospital, Naval Medical University, 168 Changhai Road, Shanghai, China. [2]GeneQuantum Healthcare (Suzhou) Co., Ltd., Buliding D, 398 Ruoshui Str., Suzhou Industrial Park, Suzhou, China. [3]GeneQuantum Medicine (Suzhou) Co., Ltd., Buliding 4, Fumin III Plant, No. 818 Wusong Road, Wuzhong District, Suzhou, China. [4]Department of Breast and Urological Medical Oncology, Fudan University Shanghai Cancer Center; Department of Oncology, Shanghai Medical College, Fudan University, 270 Dong'an Road, Shanghai, China. [5]Department of Medical Oncology, Senior Department of Oncology, The Fifth Medical Center of PLA General Hospital, 8 Dongdajie Road, Fengtai District, Beijing, China. [6]These authors contributed equally: Lei Huang, Gang Qin, Chengcheng Gong, Yajun Sun. ✉e-mail: qing@genequantum.com; paul@genequantum.com; shiy@genequantum.com; shill@genequantum.com; yangbo@301hospital.com.cn; wangbiyun0107@hotmail.com

https://doi.org/10.1038/s41467-025-64675-6

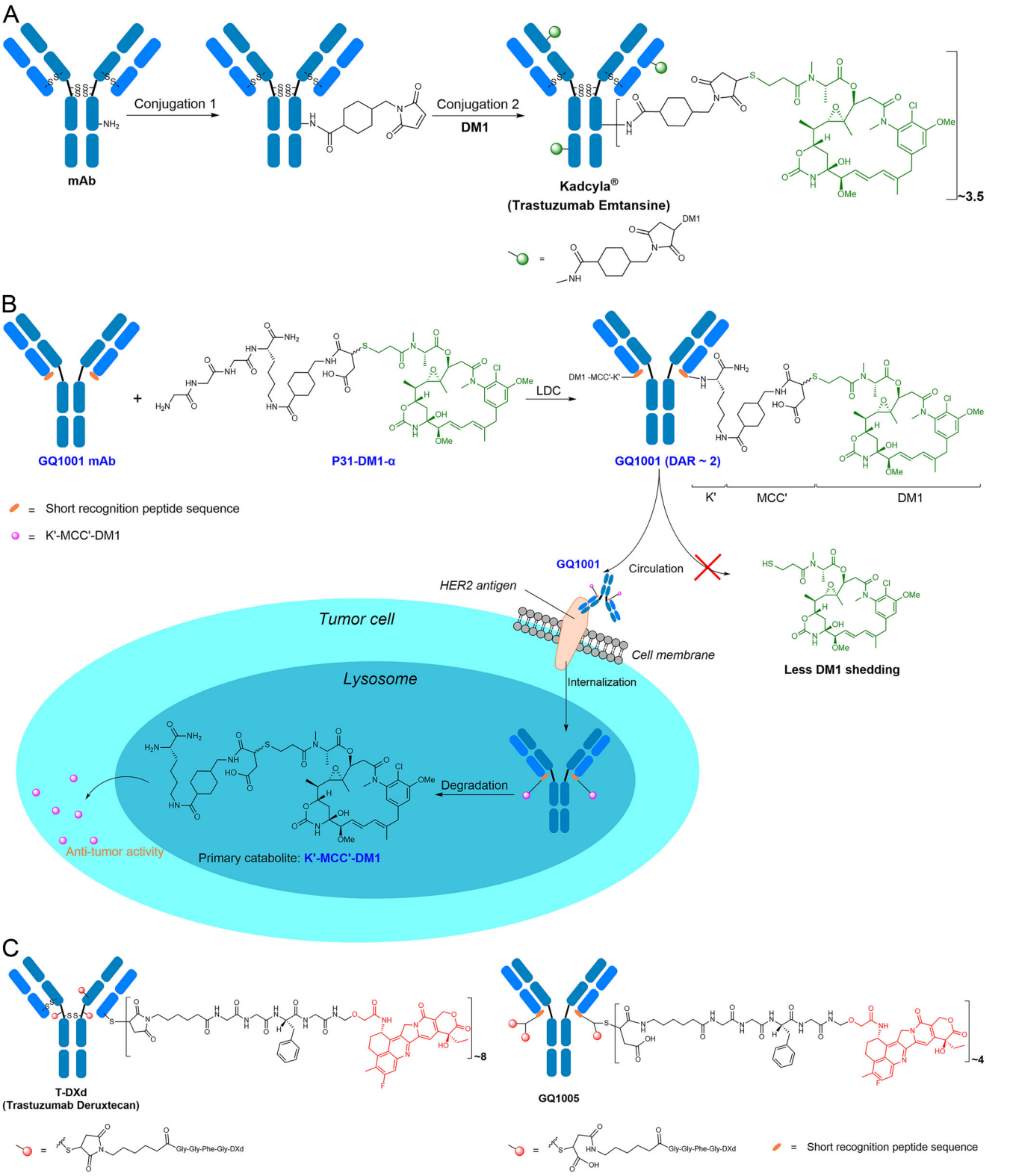

Fig. 1 | Chemical structure and catabolism. A Application of the thiosuccinimide structure in the antibody-drug conjugate Kadcyla® (trastuzumab-emtansine, T-DM1). While lysine residues-based conjugation is applied for T-DM1, Michael-addition reaction between sulfhydryl and maleimide remains used in the second conjugation reaction, which also produces thiosuccinimide structure fragments. **B** Design, production, and catabolism pathway of GQ1001. GQ1001 is designed with a stable thiosuccinimide ring-opening linker site-specifically linking DM1 to HER2 antibody via streamlined ligase-dependent conjugation (LDC) sorting, which avoids the presence of the thiosuccinimide structure in the final antibody-drug conjugate (ADC). The linker-payload P31-DM1-α is site-specifically conjugated to the C-terminal of the HER2 antibody using the robust LDC platform to generate a next generation ADC, the highly stable, homogenous GQ1001. When administrated, GQ1001 is highly stable in circulation, and is delivered to the target tumor in a highly specific manner. Then it is internalized into the tumor cells, undergoes trafficking into the lysosome for degradation, and releases the active metabolites, mainly K′-MCC′-DM1, thereby killing tumor cells. mAb, monoclonal antibody; DAR, drug-to-antibody ratio. **C** Design of T-DXd (left) and GQ1005 (right).

Michael reaction or sulfhydryl group exchange with endogenous mercaptans including serum albumin and glutathione, which leads to premature systemic shedding of toxins or linker-toxins from the ADC. Notably, Enhertu® (trastuzumab-deruxtecan, T-DXd), a recent notable ADC, is relatively stable in vivo compared with other ADCs[3].

The released toxins or linker-toxins in either the free-drug or albumin-drug conjugate format are likely to cause off-target toxicities in normal tissues via non-specific delivery. ADC homogeneity harbors a critical significance in maximizing therapeutic efficacy[4]. Besides the higher risks of premature drug release, the cysteine-maleimide-based conjugation can also cause ADC heterogeneity, particularly for ADCs with unsaturated conjugation (a broad drug-to-antibody ratio (DAR) distribution of 0-8 can be generated). This is believed to introduce a negative impact on the stability, therapeutic efficacy, safety profile, pharmacokinetics, and immunogenicity of the ADCs.

The abovementioned thiosuccinimide-associated instability and ADC heterogeneity, both arising from traditional stochastic conjugation, are a major reason for various problems of traditional ADCs, including weakened efficacy and increased off-target toxicities with narrow therapeutic-window related to higher exposure to released-drugs in plasma[5]. In clinical trials of HER2-targeting ADCs, several dose-limiting toxicities including interstitial pneumonia[6–8], thrombocytopenia, neutropenia, and neuropathy were observed, and some might be associated with free-drugs in plasma; for T-DM1, released DM1 was well-detectable in circulation[9–12]. An improved linker system with enhanced safety-profile is highly desired.

In recent years, researchers have been painstakingly investigating the physicochemical properties of thiosuccinimide structure, and found that under specific conditions, it could undergo hydrolytic ring-opening reaction and convert into succinic-acid structure, which could avoid the retro-Michael and mercapto-exchange reactions to a large extent, greatly enhancing linker stability with reduced toxicity[13–15]. However, this strategy takes advantage of post-conjugation hydrolysis, and also has various disadvantages, including difficult antibody engineering and greater heterogeneity partly due to lack of purification method.

To tackle the problem of instability with thiosuccinimide structures and high heterogeneity with traditional random-conjugation, we developed a unique kind of advanced stable linker, and a one-enzyme, one-step site-specific conjugation technology based on enzyme immobilization termed ligase-dependent conjugation (LDC) was applied for developing GQ1001 and GQ1005. Both ADCs are designed with stable thiosuccinimide ring-opening linker site-specifically linking DM1 and DXd, respectively, to HER2 antibody via streamlined LDC sorting (Fig. 1B), which avoids the presence of the thiosuccinimide structure in the final ADC. Both ADCs have great potential to minimize premature drug release and off-target toxicity associated with retro-Michael reaction and high heterogeneity that is commonly observed in conventional ADCs based on Cys-Mal conjugation.

Moreover, the pretreatment with or in concurrent use of tyrosine kinase inhibitors (TKIs) against the ADC target HER2 in addition to ADC can stimulate HER2 internalization and thus significantly enhance the endocytosis and anticancer activity of HER2-targeting ADCs[16–20]. Also, the efficacy of HER2-targeting ADCs is challenged by the occurrence of resistance to these agents[21–25].

In this work, we demonstrate that the LDC technology and ring-opening linker significantly improve the stability, safety, and pharmacokinetics in GQ1001 (modified from T-DM1) and GQ1005 (modified from T-DXd) when compared with similar ADCs, with mostly similar anticancer efficacies in various preclinical models. Importantly, given the promising linker stability of GQ1001 and GQ1005, substantially lower free DM1 and DXd exposure and lower toxicity than other similar ADCs are observed in animal models including monkeys. GQ1001 and GQ1005 effectively suppress several cancers not responsive to multiple therapeutics including those targeting HER2. When further exploring the possible clinical use settings of GQ1001, an ADC developed applying the LDC technology and the stable ring-opening linker with reduced toxicity, the anticancer efficacy of GQ1001 is significantly enhanced by HER2-targeting TKIs or by systemic chemotherapeutic agents and/or monoclonal antibodies. We also show that in cancers resistant to T-DXd due to high expression of ABCG2[26–28], GQ1001 is still efficacious. These all support the potential of GQ1001 and GQ1005 to address the unmet medical needs in HER2-positive cancer patients.

Results

Structural design, preparation, and characterization of GQ1001

For overall design of GQ1001, LDC technology was applied to confer the conjugation site specificity. A short recognition peptide sequence was introduced into the C-terminal of the light chain of trastuzumab, which did not significantly affect HER2 binding of the antibody, but offered an optimal attachment site for the cytotoxic payload DM1. To overcome the instability of conventional ADC, a uniquely-designed stable linker was developed. The linker-payload internally named as P31-DM1-α is a key component of GQ1001, and its core structure, C-terminal-amidated K-MCC′-DM1, mimics T-DM1's linker-payload, but has undergone thiosuccinimide ring-opening modification, which further enhances stability with premature detachment avoided. We compared GQ1001 majorly with its similar and derivative ADC, T-DM1, both with DM1 as the payload and with engineered trastuzumab as monoclonal antibody (mAb). P31-DM1-α is site-specifically conjugated to the C-terminal of the HER2 antibody using the robust LDC platform to generate a next generation ADC, the highly stable, homogenous GQ1001. When administrated, GQ1001 is highly stable in circulation, and is delivered to the target tumor in a highly specific manner. Then it is internalized into the tumor cells, undergoes trafficking into the lysosome for degradation, and releases the active metabolites, mainly K′-MCC′-DM1, thereby killing tumor cells. The design, production, and catabolism pathway of GQ1001 is illustrated in Fig. 1B.

Discrepant from other uncontrollable ring-opening strategies[13,14], ring-opening reaction in ours occurs during pre-conjugation synthesis under weak-alkaline conditions, which advantageously makes the ring-opening process more controllable and which can generate nearly 100% of ring-opening product through further purification with markedly-improved drug-forming and quality. Furthermore, after ring-opening reaction, a carboxyl group is generated in the linker, which significantly improves the hydrophilicity of P31-DM1-α. These effectively ensure that the subsequent enzyme-catalyzed conjugation can be conducted in an aqueous-phase system with little impact on antibodies. Identification of conjugation site and P31-DM1 isomers study are described in Supplementary Note 1.

GQ1001 was prepared through one-step conjugation reaction catalyzed by engineered Sortase A, which was immobilized by agarose resin and prepacked into a column (Fig. 2A). The monoclonal antibody reaction solution and the linker-payload reaction solution were separately prepared, and then pumped into the prepacked conjugation column. Through immobilized enzyme catalysis, the monoclonal antibody was conjugated with the linker-payload to form the ADC molecule, and the reaction solutions flowed through the prepacked conjugation column for continuous production of ADCs. The conjugation of ADCs was completed using the flowthrough mode. Hydrophobic interaction chromatography (HIC)-high-performance liquid-chromatography (HPLC) analysis showed that GQ1001 had high homogeneity with 99% of components harboring a DAR of 2 (Fig. 2B). The conjugation site could be accurately identified by the peptide-mapping method (Supplementary Fig. 1). Size-exclusion chromatography also showed that GQ1001 had high purity with monomer proportion greater than 99% (Fig. 2C). The stability test showed that the quality and biological activity of GQ1001 remained essentially

https://doi.org/10.1038/s41467-025-64675-6

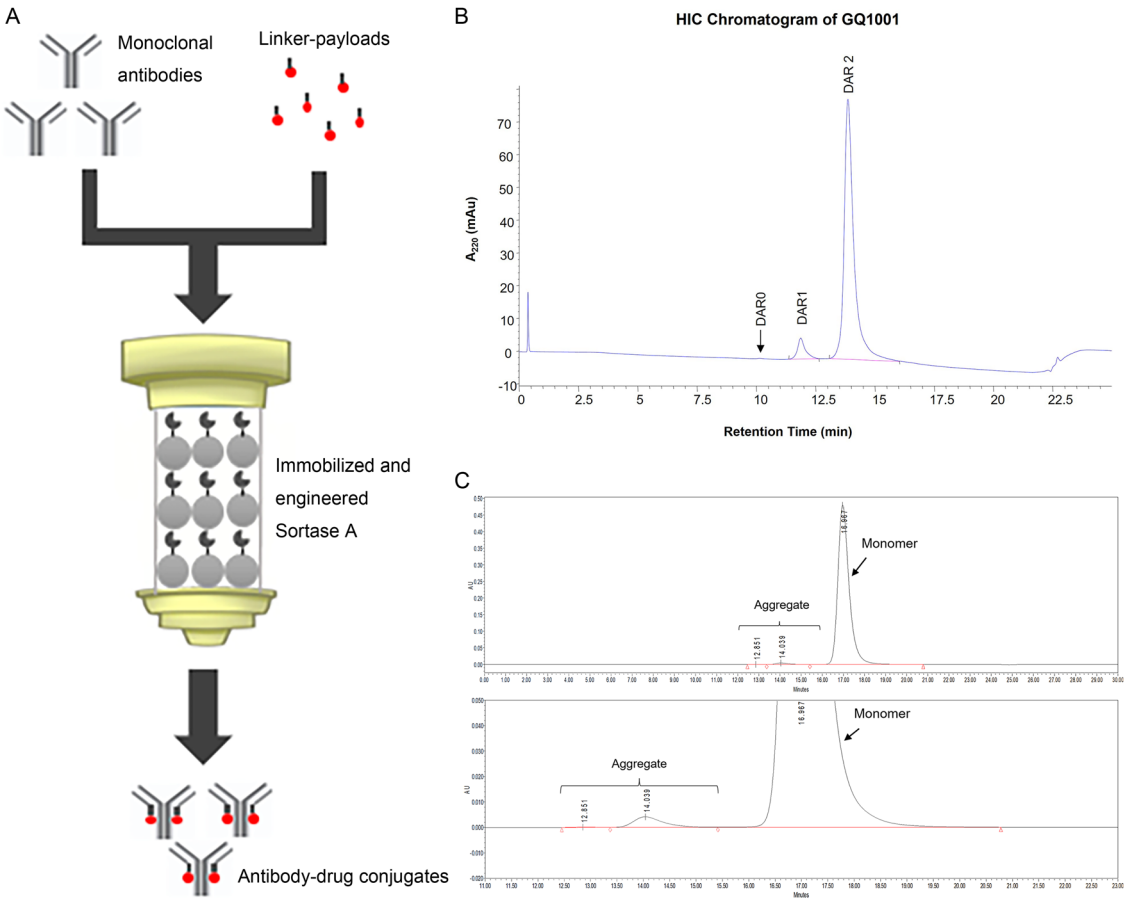

Fig. 2 | Conjugation and characterization. A Ligase-dependent conjugation (LDC) technology catalyzed by immobilized and engineered Sortase A. GQ1001 was prepared through one-step conjugation reaction catalyzed by engineered Sortase A, which was immobilized by agarose resin and prepacked into a column. The monoclonal antibody reaction solution and the linker-payload reaction solution were separately prepared, and then pumped into the prepacked conjugation column. Through immobilized enzyme catalysis, the monoclonal antibody was conjugated with the linker-payload to form the ADC molecule, and the reaction solutions flew through the prepacked conjugation column for continuous production of ADCs. **B** Drug-to-antibody ratio (DAR) distribution characterization by hydrophobic interaction chromatography (HIC)-high-performance liquid-chromatography (HPLC) analysis, which showed that GQ1001 had high homogeneity with 99% of components harboring a DAR of 2. **C** Purity based on size-exclusion chromatography, which also showed that GQ1001 had high purity with monomer proportion greater than 99%.

unchanged after 36 months of storage at 2–8 °C in buffer solution (Supplementary Table 1).

In vitro efficacy and pharmacological mechanism of GQ1001

Inhibitory effects of GQ1001 on various HER2-amplified human cancer cells (HCC1954, NCI-N87, SK-BR-3, SK-OV-3, and BT474) were remarkable and significantly greater than those of the payload, the parental monoclonal antibody (mAb), and mAb combined with P31-DM1-α (Fig. 3A and S2A-C). In HER2-amplified cancer cells, the anticancer activities of GQ1001 were slightly lower than those of T-DM1 (Fig. 3A). Up to 100 nM GQ1001 showed negligible effect on HER2-negative MDA-MB-468 cells, while T-DM1[29] demonstrated significant cytotoxicity on these cells (IC_{50}: 10.55 nM; Fig. 3A); these suggested that the efficacy of GQ1001 was more HER2-specific, and that GQ1001 might have lower off-target toxicity compared to T-DM1. The activities of T-DXd and DXd on SK-BR-3, NCI-N87, and MDA-MB-468 cells are illustrated in Supplementary Fig. 2D-F. Binding affinities, antibody-dependent cell-mediated cytotoxicity (ADCC) effect, internalization efficiency, and catabolism of GQ1001 are shown in Supplementary Tables 2-5 and Supplementary Figs. 3-5, and described in Supplementary Note 2.

For HER2-amplified cancer cells (HCC1954 and NCI-N87), proportions of cells arrested in G2/M phase after 24-h GQ1001 treatment (0.2–1.8 nM) increased in a concentration-dependent manner; however, up to 18.0 nM GQ1001 did not show a significant impact on the cycle of HER2-negative MDA-MB-468 cells, as opposed to DM1 and T-DM1 (Fig. 3B). The concentration-dependent apoptosis-promoting effects of GQ1001 as suggested by increased Caspase-3/7 activity on HCC1954 (EC_{50}, 0.23 vs 0.14 nM) and NCI-N87 (EC_{50}, 0.20 vs 0.14 nM) cells were strong and similar to those of T-DM1, while GQ1001 did not significantly induce apoptosis in HER2-negative MDA-MB-468 cells at concentration up to 100.00 nM, as opposed to T-DM1 (EC_{50}, 17.58 nM) (Fig. 3C). Together, GQ1001 might have little off-target toxicity on relatively very low HER2-expressing cells, with better safety than T-DM1.

In vivo antitumor efficacies in HER2-positive/amplified CDX and PDX models of various cancer types

Single-dose intravenous GQ1001 administration potently inhibited growth of subcutaneously-engrafted tumors in several human cancer cell-derived xenograft (CDX) mouse models in a dose-dependent manner (Fig. 4A, Supplementary Fig. 6A-B, Supplementary Tables 6-8). GQ1001 and T-DM1 mostly showed similar antitumor activities at the same doses. The minimal effective doses in different CDX models ranged from 1.25 mg/kg in breast cancer HCC1954 model to 5 mg/kg in breast cancer BT474 and gastric cancer NCI-N87 models.

GQ1001 also had potent antitumor efficacies in various patient-derived xenograft (PDX) models, the most relevant model for

https://doi.org/10.1038/s41467-025-64675-6

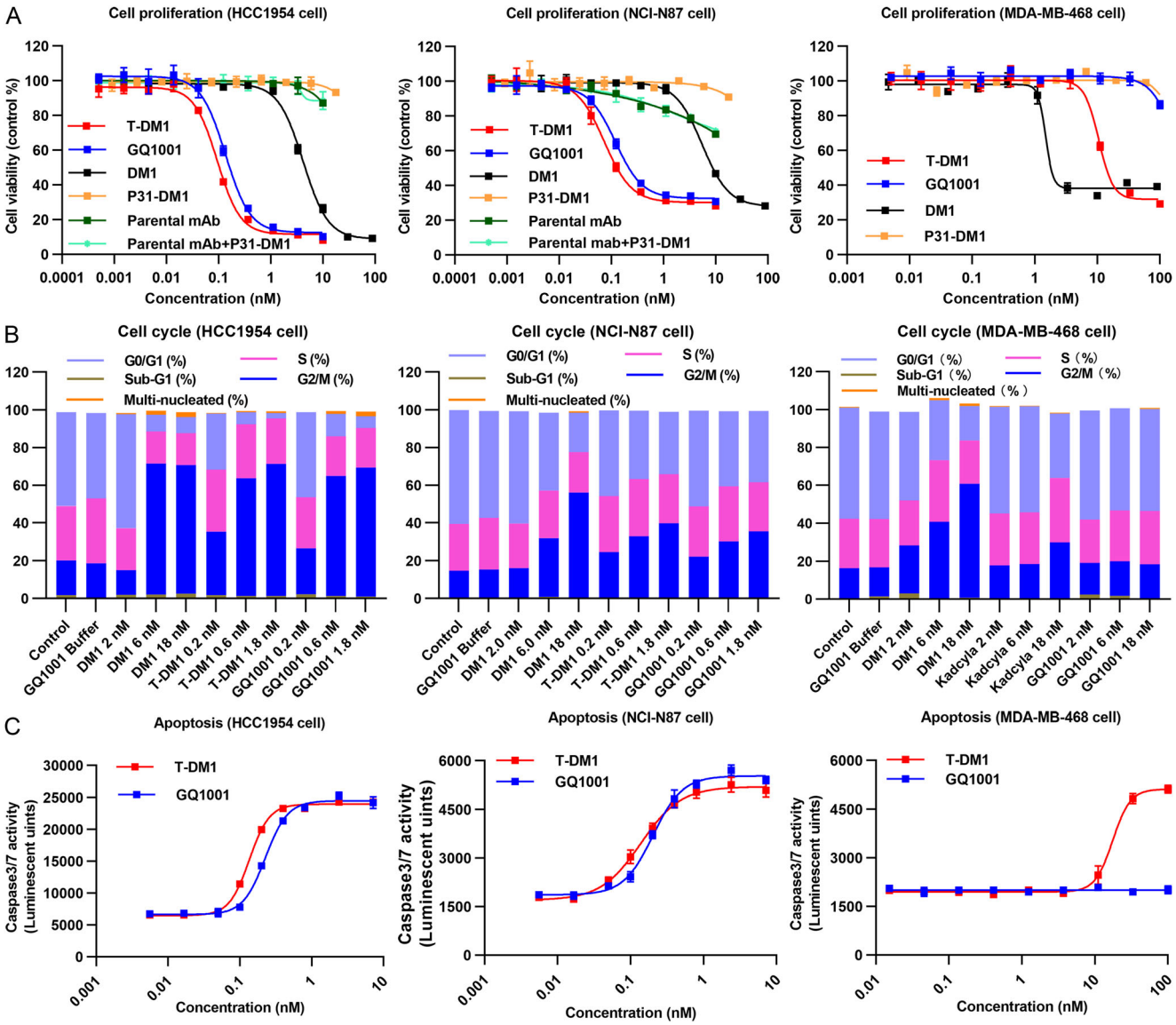

Fig. 3 | In vitro efficacy and mechanisms of action. A Fitted curves for the in vitro inhibitory effects of GQ1001, T-DM1, and controls on the viability and proliferation of HER2-overexpressing (HCC1954 and NCI-N87) and HER2-negative (MDA-MB-468) cancer cells using CellTiter-Glo® Luminescent Cell Viability Assay. Inhibitory effects of GQ1001 on HER2-amplified human cancer cells were remarkable and significantly greater than those of the payload, the parental monoclonal antibody (mAb), and mAb combined with P31-DM1-α. In HER2-amplified cancer cells, the efficacies of GQ1001 were slightly lower than those of T-DM1. Importantly, up to 100 nM GQ1001 showed negligible effect on HER2-negative MDA-MB-468 cells, while T-DM1 demonstrated significant cytotoxicity on these cells (IC50: 10.55 nM). (**B**) Cell cycle and (**C**) apoptosis (measured by activation of Caspase-3/7) of HER2-amplified and HER2-negative cancer cells. **A**–**C** performed three times. For HER2-amplified cancer cells (HCC1954 and NCI-N87), proportion of cells arrested in G2/M phase after 24-h GQ1001 treatment (0.2–1.8 nM) increased in a concentration-dependent manner; however, up to 18.0 nM GQ1001 did not show a significant impact on the cycle of HER2-negative MDA-MB-468 cells, as opposed to DM1 and T-DM1. The concentration-dependent apoptosis-promoting effects of GQ1001 as suggested by increased Caspase-3/7 activity on HCC1954 (EC_{50}, 0.23 vs 0.14 nM) and NCI-N87 (EC_{50}, 0.20 vs 0.14 nM) cells were strong and similar to those of T-DM1, while GQ1001 did not significantly induce apoptosis in HER2-negative MDA-MB-468 cells at concentration up to 100.00 nM, as opposed to T-DM1 (EC_{50}, 17.58 nM). For curves in **A**, **C** means and standard errors are shown. Source data are provided as a Source Data file.

patients[30]. The LD2-0017-201149 and ST-02-0318 models originated from surgical samples of HER2 IHC 3+ and 2+ gastric cancer, respectively. The CTG-0927 model was derived from an intrahepatic-cholangiocarcinoma patient with high HER2-expression based on NGS who had been previously treated with cisplatin plus gemcitabine without response, gemcitabine plus docetaxel plus capecitabine with response, poly-ADP-ribose polymerase (PARP)-inhibitor without response, and 5-fluorouracil plus irinotecan also without response. The LD1-0038-361855 model came from the resected specimen of a patient with HER2 IHC 3+, moderately-differentiated, rectal tubular adenocarcinoma with liver metastasis. The LD1-0006-217643 model originated from the resected tumor specimen of a patient with HER2 IHC 2+, primary bronchogenic adenocarcinoma of the middle lobe of right lung. Single- or double-dose GQ1001 demonstrated strong anti-tumor activities in all the above PDX models in a dose-dependent manner (Fig. 4B-E, Supplementary Fig. 6C, Supplementary Tables 9-13).

In the LD1-0038-361855 colorectal cancer PDX model (Fig. 4D), GQ1001 had slightly inferior anticancer efficacy compared to T-DXd at 10 mg/kg single dose. In the LU-01-1626 non-small cell lung cancer PDX model (exon20 ins, HER2 1+; Fig. 4F), GQ1001 had an anticancer efficacy comparable to T-DXd when administered at 10 mg/kg on Days 0 and 14.

https://doi.org/10.1038/s41467-025-64675-6

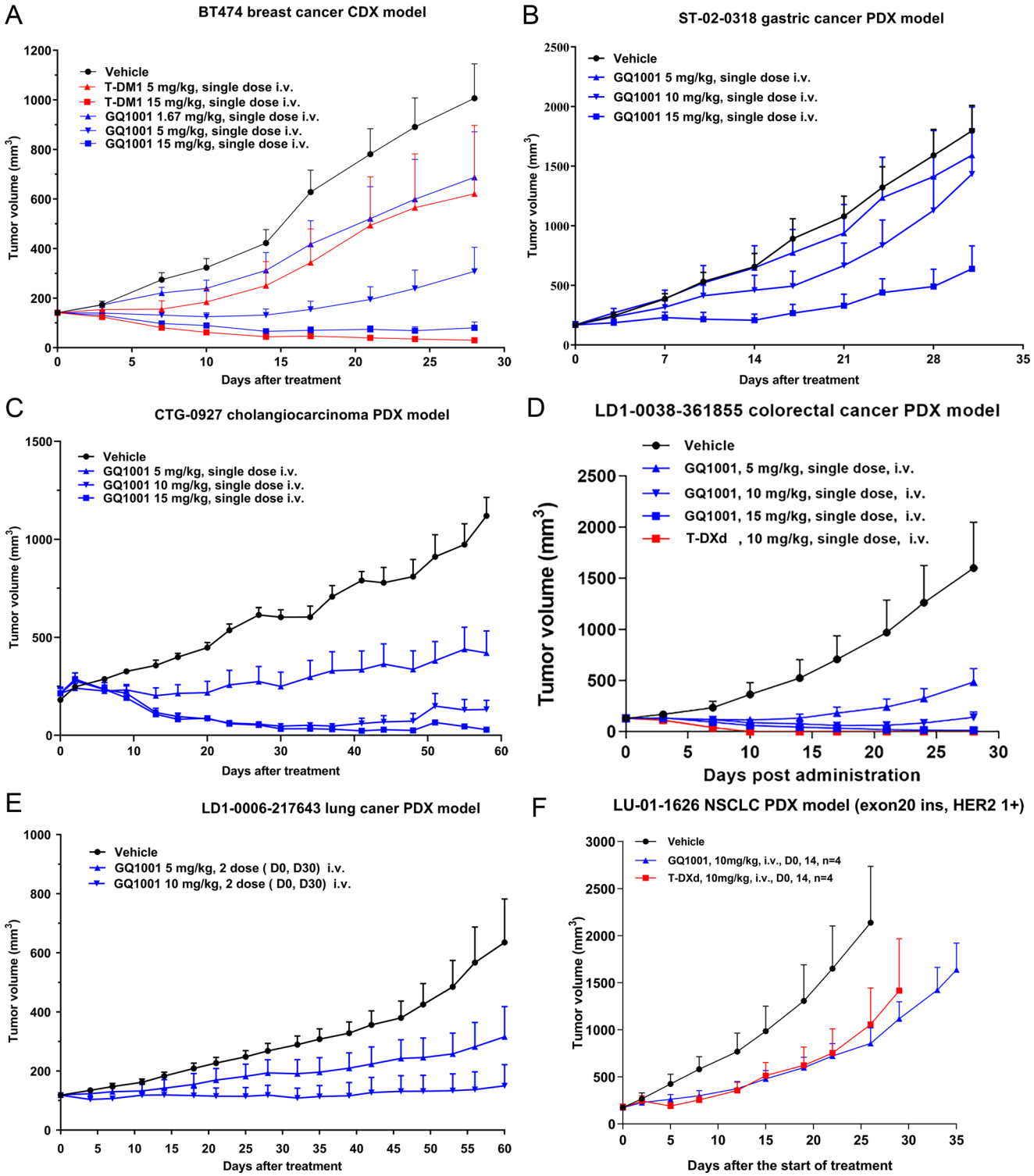

Fig. 4 | Dose-dependent in vivo anticancer efficacies. Tumor growth curves (tumor sizes over time) showing the in vivo anticancer efficacies of different concentrations of GQ1001 (versus T-DM1 or T-DXd) in HER2-amplified human cancer cell-derived xenograft (CDX) and patient-derived xenograft (PDX) tumor models of female nude BALB/c mice. **A** Breast cancer BT-474 CDX model ($n = 10$ per group; single-dose): Single-dose intravenous GQ1001 administration potently inhibited growth of subcutaneously-engrafted tumors in the human cancer CDX mouse model in a dose-dependent manner; **B** gastric cancer ST-02-0318 PDX model ($n = 5$ per group; single-dose), **C** cholangiocarcinoma CTG-0927 PDX model ($n = 5$ per group; single-dose), **D** colorectal cancer LD1-0038-361855 PDX model ($n = 5$ per group; single-dose), and (**E**) lung cancer LD1-0006-217643 PDX model ($n = 5$ per group; repeated doses on Days 0 and 30): Single- or double-dose GQ1001 demonstrated strong antitumor activities in all the above PDX models in a dose-dependent manner. In the LD1-0038-361855 colorectal cancer PDX model, GQ1001 had slightly inferior anticancer efficacy compared to T-DXd at 10 mg/kg single dose; (**F**) non-small cell lung cancer LU-01-1626 PDX model (exon20 ins, HER2 1+; $n = 4$ per group; repeated doses on Days 0 and 14): GQ1001 had an anticancer efficacy comparable to T-DXd when administered at 10 mg/kg. Regimens and doses are detailed within the subfigures. Datapoints represent group mean of tumor size, and error bars represent standard deviation of the mean. Statistical tests used and exact p-values are provided in Supplementary Tables 6 and 9–12, on the figures themselves, and/or in the Source Data file. Source data are provided as a Source Data file. i.v., intravenous.

These findings strongly suggested that GQ1001 innovatively developed using GeneQuantum LDC technology might be clinically applicable despite lower DAR, and displayed efficient anticancer effects in HER2-expressing tumors including those heavily-pretreated.

Efficacy of GQ1001 in cancers with high ABCG2 expression resistant to T-DXd

In cancers resistant to T-DXd due to high ABCG2 expression, GQ1001 was still efficacious. In vitro experiments suggested that DXd was a stronger substrate of ABCG2, while DM1 and the major metabolite of GQ1001, K′-MCC′-DM1, were not major ABCG2 substrates (Supplementary Fig. 7), which are in line with literatures[26–28]. In ABCG2-highexpressing cancer cell lines (NCI-H2110 and Caco-2), the IC_{50} for cell viability was markedly lower with DM1 than with DXd; the addition of the ABCG2 inhibitor YHO-13351 did not meaningfully change the IC_{50} in cells treated with DM1, MCC′-DM1, or K′-MCC′-DM1, while it markedly decreased the IC_{50} in DXd-treated cells, supporting that DXd but not DM1 resistance is dependent on ABCG2. In vivo experiments showed that in the NCI-N87 cancer CDX model overexpressing ABCG2, GQ1001 exhibited significantly better pharmacological effects than T-DXd, and that the ABCG2 inhibitor YHO-13351 enhanced the sensitivity of cancer to T-DXd (Supplementary Fig. 6D). These findings suggest that cancers with high expression of ABCG2 are resistant or insensitive to T-DXd, while GQ1001 can overcome ABCG2-mediated treatment resistance and bring greater benefits to patients with ABCG2-overexpressing cancer.

Pharmacokinetics of GQ1001 in SD-rats and cynomolgus-monkeys

After single intravenous infusion of GQ1001 (6, 20, 60, and 90 mg/kg) in SD rats and repeated intravenous infusion of GQ1001 (10, 30, and 45 mg/kg) in cynomolgus-monkeys (Fig. 5A-F, Supplementary Tables 14-15), serum GQ1001 and TAb concentrations peaked rapidly and declined in a roughly-biphasic manner; DM1 concentrations were at least 3000-fold lower (on a molar basis) than GQ1001 at all times in both rats and monkeys. Mean C_{max} and $AUC_{0\text{-}t}$ of GQ1001, TAb, and DM1 increased with increasing GQ1001 dose. No apparent drug accumulation was noted after repeated doses.

Notably, after intravenous infusion of 60 mg/kg GQ1001 in SD-rats, mean C_{max} of the toxin payload DM1 was only 1.84 ng/mL, which was only 1.32% of that for T-DM1[12] (Fig. 5G); after intravenous infusion of 30 mg/kg GQ1001 in cynomolgus-monkeys, for the first 3 cycles of administration, percentages of DM1 C_{max} for GQ1001 were much smaller than (~ 1/100 of) those for T-DM1[12] (Fig. 5H). After intravenous infusion of GQ1001 into cynomolgus-monkeys, DM1 was only detectable at low levels within 4 h (45 mg/kg group, C_{max}, ~1 ng/mL); while for T-DM1, DM1 was stably detectable until 7 days (30 mg/kg group, C_{max}, ~65 ng/mL), with area under curve (AUC) more than 500,000 folds of that of GQ1001 (Fig. 5H)[31].

Plasma stability experiments showed that the in vitro concentrations of free DM1 in buffer and from GQ1001-treated rat, monkey, and human plasmas increased slowly after administration, and were markedly lower than those in T-DM1-treated monkey and human plasmas at all measured timepoints. Concentrations of free DM1 detected in GQ1001-treated plasmas of all species were ~2 ng/mL at 0 h, and rose to nearly 10 ng/mL at 96 h; while the concentrations in T-DM1-treated plasmas were ~80 ng/mL at 0 h, and increased to nearly 2000 ng/mL at 96 h (Fig. 5I). At 96 h, DM1-shedding ratio of GQ1001 in human plasma was only about 1/100 of that of T-DM1 (0.11% vs 11.84%).

These results suggested that circulation DM1 level of GQ1001 was markedly lower than that of T-DM1, and supported the great stability of the modified ring-opening linker in GQ1001. It is anticipatable that DM1-associated side-effects from GQ1001 would be much fewer than those from T-DM1.

Toxicities of GQ1001 in cynomolgus-monkeys, rats, and mice

Toxicity findings are detailed in Supplementary Note 3 and herein briefly summarized. 7-week repeated-dose toxicity study of GQ1001 was carried out in cynomolgus-monkeys. After intravenous administration, all animals survived until their scheduled necropsy. No drug-related changes in bodyweight, food consumption, clinical observation, body temperature, ophthalmology examination, cardiovascular/respiratory/central nervous system function, immunophenotypes, urinalysis, or gross pathology were noted in any animal. Overall, toxicity of GQ1001 was significantly less and milder than T-DM1, with no toxicity severity beyond that of T-DM1. Main toxicities of GQ1001 in monkeys were only hepatic (dose-dependent elevation of ALT and AST levels), platelet (dose-dependent decrease in platelet count), and lymphoid abnormalities (mainly spleen enlargement), and all the changes recovered after 4-week recovery period (Fig. 5J). However, for T-DM1, besides the aforementioned adverse-events, there are still other severe ones including lymphoid depletion in spleen and thymus, mononuclear cell infiltration in interstitium of lungs, and axonal degeneration in spinal cord and sciatic nerve (Supplementary Table 16)[12,31], with some pathological abnormalities like axonal degeneration still not recovered at the end of 6-week recovery period.

In cynomolgus-monkeys the highest non-severely-toxic-dose (HNSTD) was 45 mg/kg, equal to 15 mg/kg in humans, for 3-time repeated administrations of GQ1001, which was markedly higher than that for 4-time repeated administrations of T-DM1 (10 mg/kg in monkeys)[12]. These indicated that GQ1001 had much better safety profile than T-DM1. Single-dose toxicity studies and key conclusions in ICR-mice, SD-rats, and cynomolgus-monkeys are shown in Fig. 5K. GQ1001 was well-tolerated in all the animals at all doses, with no mortalities observed. In SD-rats and cynomolgus-monkeys, there were no severe adverse-events noted and almost all the observed abnormities recovered at study end. Even at dose up to 300 mg/kg in ICR-mice, equal to 25 mg/kg in humans, still no severe toxicities were noted.

The highly superior safety profile of GQ1001 with very low level of released toxin payload compared with similar ADC suggested that GQ1001 might markedly expand the clinical therapeutic index, which might improve quality of life for patients while ensuring efficacy.

Supra-additive anticancer efficacies of GQ1001 combined with HER2-targeting TKIs and chemotherapy with/without pertuzumab in various HER2-positive tumor CDX and PDX models

TKIs present powerful antitumor activity with antitumor mechanism different from that of GQ1001, and combination of these two different therapeutics was anticipated to introduce supra-additive antitumor activity. We investigated efficacy of GQ1001 combined with HER2-targeting TKIs (pyrotinib, tucatinib, and neratinib)[32] in gastric cancer and breast cancer (with bone or brain metastasis) PDX models (Figs. 6 & 7A-C, Supplementary Tables 17-23).

In the LD2-0017-201149 and ST-02-0103 gastric cancer PDX models, GQ1001 combined with tucatinib or pyrotinib showed supra-additively enhanced anticancer effects. In the LD2-0017-201149 model, endpoint analysis showed that tumor size was smaller in the T-DXd group compared with the GQ1001-tucatinib combination group on Day 35, before which there was a cross between the tumor growth line of the T-DXd group and that of the GQ1001-tucatinib combination group (Fig. 6A; Supplementary Table 17); GQ1001 combined with pyrotinib showed an anticancer efficacy similar to T-DXd (Fig. 6B; Supplementary Table 17). Excitingly, combination of GQ1001 with pyrotinib caused complete response (CR) in all animals of the LD2-0017-201149 model. These suggested that GQ1001 combined with TKIs could bring good efficacy to patients with strongly-heterogenetic gastric cancer[33,34] (Fig. 6A-C).

Single- or repeated-dose GQ1001 combined with tucatinib, pyrotinib, or neratinib also demonstrated supra-additive anticancer

https://doi.org/10.1038/s41467-025-64675-6

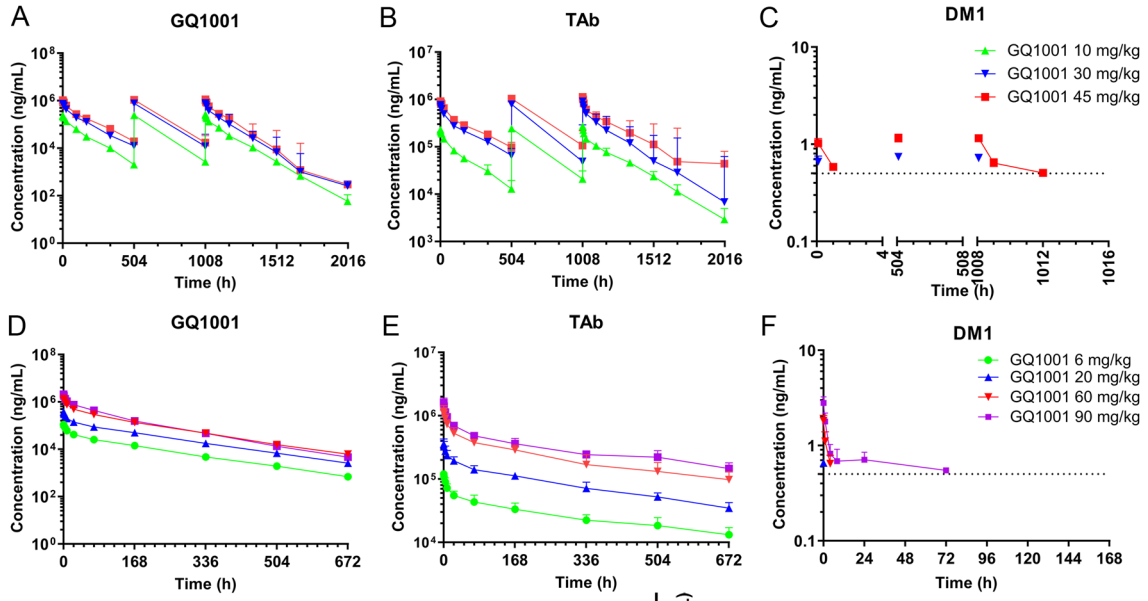

G

Sex	GQ1001 60 mg/kg			T-DM1 60 mg/kg*		
	Mean	SD	n	Mean	SD	n
C_{max} (ng/mL) of DM1 in rat						
Male	1.66	0.151	3	124	12.9	10
Female	2.02	0.137	3	154	13.9	10

H

Sex	GQ1001 30 mg/kg			T-DM1 30 mg/kg**		
	Mean	SD	n	Mean	SD	n
C_{max} (ng/mL) of DM1 in monkey						
Male	0.719	0.0119	5	61.8	0.755	4
Female	0.725	0.0922	5	66.0	4.780	4
AUC (day*ng/mL) of DM1 in monkey						
Male	0.0012542	0.0001171	5	53.7	14.20	4
Female	0.0010500	0.0001121	5	65.1	9.66	4

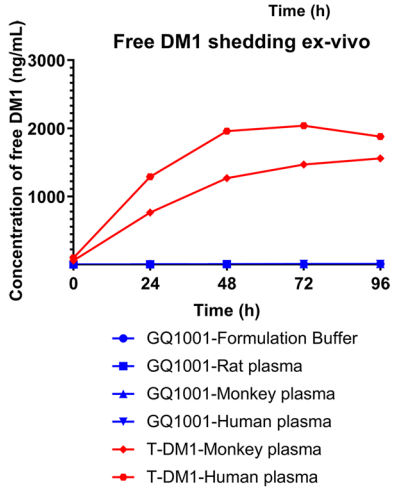

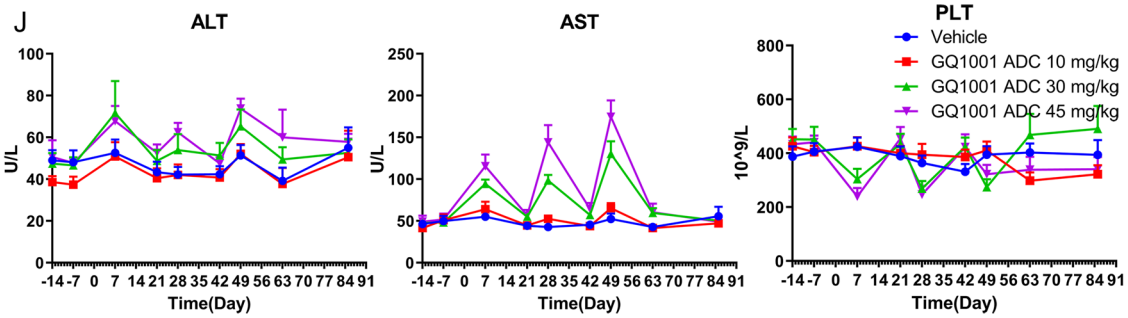

K

Study	Dosing schedule	Key conclusion
Single-dose toxicity in ICR mice	90, 165, 240, and 300 mg/kg; iv	MTD =300 mg/kg
Single-dose toxicity in SD rats	20, 60, and 120 mg/kg; iv	MTD >120 mg/kg
Single-dose toxicity in cynomolgus monkeys	10, 30, and 45 mg/kg; iv	MTD >45 mg/kg
Repeated-dose toxicity in cynomolgus monkeys	10, 30, and 45 mg/kg; iv, Q3W × 3	HNSTD =45 mg/kg

activity, similar to T-DXd[35,36] in the BR050 (HER2 + ++ breast infiltrating ductal carcinoma) PDX model (Fig. 6D-F). In cases with breast cancer resistant to pyrotinib (LD1-2009-362721 PDX model) and those with heavy tumor metastasis burden (LD1-2009-361973, bone metastasis; LD1-2009-362541, brain metastasis), combo treatment of GQ1001 with tucatinib or pyrotinib still exhibited good supra-additive antitumor activity (Fig. 7A-C). These indicated that GQ1001 combined with TKIs could be treatment options for such cancer patients, including those resistant to TKIs.

In addition to the supra-additive effects when in combination with TKIs, GQ1001 has also demonstrated good improved antitumor effects when used with chemotherapeutic agents and/or HER2-targeting

Fig. 5 | Pharmacokinetics analyses after single-dose GQ1001 administration in SD rats and during repeated-dose GQ1001 administration in cynomolgus monkeys, plasma stability, and toxicity of GQ1001. Concentrations of (**A**) GQ1001, **B** total antibody (TAb), and (**C**) free DM1 following single-dose GQ1001 administration at 6, 20, 60, and 90 mg/kg in SD rats ($n = 10$ per group). Concentrations of (**D**) GQ1001, **E** total antibody, and (**F**) free DM1 following repeated-dose GQ1001 administration (on Days 1, 22, and 43) at 10, 30, and 45 mg/kg in cynomolgus monkeys ($n = 6$ per group). **G** Comparison of C_{max} of free DM1 between GQ1001- and T-DM1-treated SD rats at 60 mg/kg. Mean C_{max} of DM1 was 1.84 ng/mL (1.32% of that for T-DM1). (**H**) Comparison of C_{max} and area under the curve (AUC) of free DM1 between GQ1001- and T-DM1-treated cynomolgus monkeys at 30 mg/kg. For the first 3 cycles of administration, percentages of DM1 C_{max} for GQ1001 were ~1/100 of those for T-DM1. For GQ1001, DM1 was detectable at low levels within 4 h (45 mg/kg group, C_{max}, ~1 ng/mL); for T-DM1, DM1 was stably detectable until 7 days (30 mg/kg group, C_{max}, ~65 ng/mL), with area under curve more than 500,000 folds of that of GQ1001. **I** In vitro plasma stability of GQ1001 as indicated by free DM1 level in plasma of various species, compared to T-DM1. At 96 h, DM1-shedding ratio of GQ1001 in human plasma was only about 1/100 of that of T-DM1 (0.11% vs 11.84%). **J** Mean levels of alanine aminotransferase and aspartate aminotransferase, and platelet count over time following repeated-dose administration (Days 1, 22, and 43) of GQ1001 (10, 30, and 45 mg/kg) and vehicle control in cynomolgus monkeys ($n = 10$ per group). All changes recovered after 4-week recovery-period. **K** GQ1001 toxicity study summary. In Fig. 5A-5H & 5J, data are presented as mean values with standard deviations. Source data are provided as a Source Data file. *Data obtained from Poon KA et al. (PMID: 24035823). **Data obtained from FDA, Center for drug evaluation and research, Application number: 125427Orig1s000, Pharmacology Review(s), (https://www.accessdata.fda.gov/drugsatfda_docs/nda/2013/125427Orig1s000TOC.cfm). MTD, maximum tolerated dose; HNSTD, highest non-severely toxic dose; iv, intravenous.

monoclonal antibodies. In the LD1-2009-362721 and BR050 breast cancer PDX model, GQ1001 combined with pertuzumab and chemotherapy (paclitaxel or capecitabine) showed better antitumor activity than triple combination treatment with trastuzumab, pertuzumab, and chemotherapy (TPH), the current standard first-line regimen for HER2-positive breast cancer (Fig. 7D-E, Supplementary Tables 24-25). Furthermore, GQ1001 combined with chemotherapy also had better efficacy than TPH treatment in the HCC1954 CDX model[10,37] (Fig. 7F, Supplementary Table 26).

Together, GQ1001 has good therapeutic potential against HER2-positive cancers when combined with TKIs or with chemotherapeutic drugs and/or monoclonal antibodies.

Application of the LDC technology and stable ring-opening linker in GQ1005

To further support that the innovative application of the LDC technology and the stable ring-opening linker could meaningfully improve the safety of ADC, preclinical data on GQ1005 are herein reported. GQ1005 with stable linker was derived from T-DXd with cysteine-succinimide linker, and GQ1005 and T-DXd shared the same mAb (engineered trastuzumab) and toxin payload (DXd) (Fig. 1C); we majorly compared GQ1005 with T-DXd. Conjugation was irreversible for GQ1005 while reversible for T-DXd.

Using the highly accurate liquid chromatography-mass spectrometry (LC-MS) method, GQ1005 demonstrated improved stability both ex vivo in plasma and in vivo in circulation when compared to T-DXd, whose DAR dropped significantly with longer time (Fig. 8A-B). The DAR of GQ1005 remained highly stable in the plasma of SD rat, cynomolgus monkey, and human; in contrast, the DAR of T-DXd significantly dropped to around 50% after 96 h of incubation in human plasma (Fig. 8A). In cynomolgus monkeys after a single dose, GQ1005 also maintained a relatively stable DAR; however, T-DXd experienced a roughly 50% reduction in DAR in circulation within one week (Fig. 8B), which is consistent with a previous report[3], and which could be due to the Michael addition reaction between the maleimide group on the linker and the thiol group on the reduced cysteine of the antibody. The resulting thiol-linked succinimide is unstable in plasma, and prone to reverse Michael addition or substitution by other thiol groups, leading to the detachment of the linker-DXd during incubation. These suggest that GQ1005 is more stable than T-DXd in human plasma.

In HER2-positive NCI-N87 human gastric cancer-bearing BALB/c nude mice, GQ1005 demonstrated higher enrichment efficiency in tumor compared with T-DXd. Despite lower DAR, GQ1005 demonstrated high payload enrichment in tumor comparable to T-DXd, but had markedly lower exposure of the toxin payload DXd in plasma than T-DXd (AUC, 3.34 vs 22.1 h*ng/mL). The tumor-to-plasma payload exposure ratio for GQ1005 with enhanced linker stability was markedly higher than that for T-DXd (AUC, 198.5:1 vs 39.7:1; Fig. 8C-D).

In pharmacokinetic/toxicokinetic studies in cynomolgus monkeys, similar with the situations for GQ1001, exposures of GQ1005, TAb, and DXd increased with higher GQ1005 dose after intravenous infusion of single-dose (10, 30, and 90 mg/kg) and repeated-dose (10, 30, and 60 mg/kg) GQ1005. The concentrations of GQ1005 ADC and TAb for most individuals peaked at 5 min or 1 h after single-dose intravenous infusion of GQ1005, with the mean C_{max} and $AUC_{0\text{-}t}$ almost dose-proportionally increasing (Fig. 8E-F). The mean serum DXd concentration was far lower than the mean serum GQ1005 ADC concentration. DXd concentration peaked 1–24 h after intravenous infusion. The serum DXd concentration in the 10 mg/kg group measured slightly higher than the lower limit of quantification (LLOQ) or was even unmeasurable. In the 30 and 90 mg/kg GQ1005 groups, the mean C_{max} and $AUC_{0\text{-}t}$ for DXd dose-dependently increased, but remained low (Fig. 8G).

After repeated intravenous infusion of GQ1005 into cynomolgus monkeys, the blood concentrations of GQ1005 ADC and TAb rapidly peaked, and the exposure levels (average C_{max} and $AUC_{0\text{-}t}$) dose-proportionally increased. The exposure level ($AUC_{0\text{-}t}$) of GQ1005 ADC after repeated administration was similar to that after the first administration, indicating no apparent drug accumulation after repeated administrations. After repeated administrations, the half-life $t_{1/2}$ of GQ1005 ADC (4.04 to 6.65 days) and TAb (6.59 to 10.20 days) was comparable to that after the first administration (Fig. 8H-I). After the first and last administration, DXd was only detectable at certain timepoints in the 10 mg/kg GQ1005 group. With increasing dose, the timepoints where DXd was detectable gradually increased in the 30 and 60 mg/kg groups, with DXd concentrations slightly higher than the LLOQ. The average C_{max} (0.291 to 0.929 ng/mL) and $AUC_{0\text{-}t}$ (41.7 to 102.0 h*ng/mL) of DXd increased with increasing dose of GQ1005 from 30 to 60 mg/kg (Fig. 8J).

Results for the toxicity studies of single-dose and repeated-dose intravenous GQ1005 infusion in cynomolgus monkeys are described in Supplementary Note 4. The MTD of GQ1005 was >90 mg/kg, and the HNSTD of GQ1005 was 60 mg/kg (versus 30 mg/kg for T-DXd), with no mortality or lung toxicity observed for GQ1005. A comparison of the in vivo safety between GQ1005 and T-DXd in cynomolgus monkeys is listed in Supplementary Table 27, supporting that GQ1005 harbored improved safety compared to T-DXd. In vitro hemolysis assay for GQ1005 showed no hemolysis or agglutination.

In vitro binding assays using ELISA showed that the binding affinity of GQ1005 mAb (engineered trastuzumab) was similar to trastuzumab (Supplementary Fig. 8A), and that the binding affinity of GQ1005 was similar to trastuzumab and T-DXd (Supplementary Fig. 8B). The internalization efficiency of GQ1005 was also similar to the parental antibody and T-DXd in different cell lines (Supplementary Fig. 8C-D). These suggested that the site-specific conjugation did not significantly impact the binding or internalization property of GQ1005.

https://doi.org/10.1038/s41467-025-64675-6

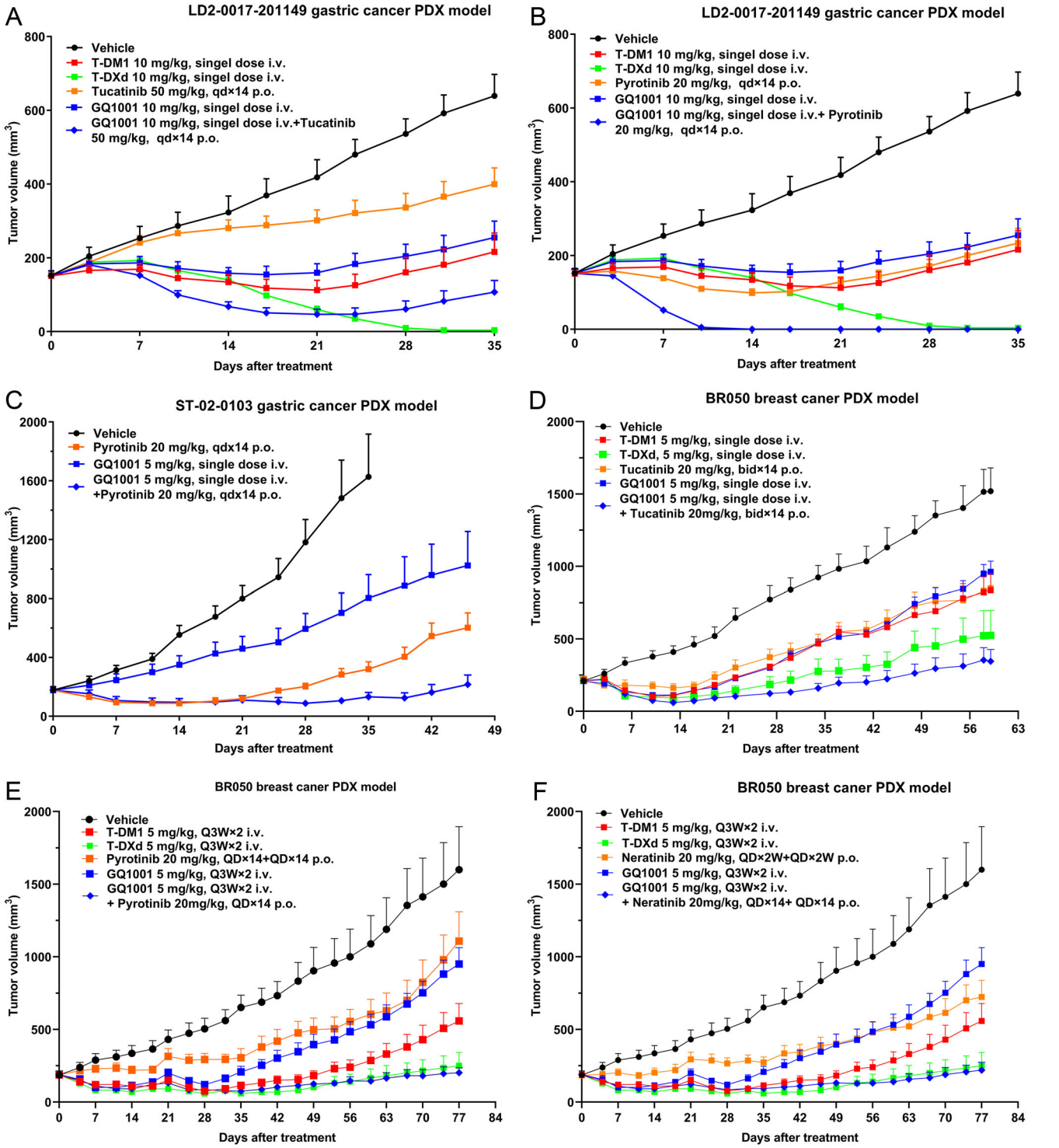

GQ1005 (DAR = 4) exhibited potent in vitro cytotoxic activities against HER2-high SK-BR-3 and NCI-N87 cancer cell lines, which were slightly weaker than T-DXd (DAR = 8) (Supplementary Fig. 8E-F). With highly stable linker, GQ1005 showed weak or no cytotoxicity in HER2-low (H2110 and CFPAC-1; Supplementary Fig. 8G-H) and HER2-negative (MDA-MB-468; Supplementary Fig. 8I) cancer cell lines even at high doses, supporting good safety profile in vitro. GQ1005 exhibited a robust bystander killing effect in vitro, which was slightly weaker than T-DXd (Supplementary Fig. 8J). GQ1005 demonstrated a stronger ADCC effect than T-DXd in a cell-based assay (Supplementary Fig. 8K), but a weaker apoptosis-inducing ability than T-DXd in HER2-high SK-BR-3 cells (Supplementary Fig. 8L). Similar to T-DXd, GQ1005 demonstrated a significant dose-dependent induction of S-phase arrest in HER2-positive HCC1954 cells, while it had no significant impact on the cell cycle of HER2-negative HepG2 cells (Supplementary Fig. 8M-N). Despite lower DAR, GQ1005 demonstrated robust dose-dependent anticancer efficacy, which was mostly comparable to T-DXd at single and repeated doses of 1, 5, and/or 10 mg/kg, across a range of HER2-positive CDX and PDX models of gastric cancer, breast cancer, pancreatic cancer, and colorectal cancer (Supplementary Fig. 9).

The overall comparison between T-DXd and GQ1005 is summarized in Supplementary Table 28, supporting less toxicity for GQ1005.

Fig. 6 | In vivo efficacies of GQ1001 combined with HER2-targeting tyrosine kinase inhibitors (TKIs), and with chemotherapy and/or HER2-targeting monoclonal antibody in multiple primary or metastatic cancers. Tumor growth curves (tumor sizes over time) showing in vivo anticancer efficacies of GQ1001 in combination with TKIs and other groups in patient-derived xenograft (PDX) mouse models: HER2-positive LD2-0017-201149 **A** single-dose GQ1001 with tucatinib, $n = 6$ per group; **B** single-dose GQ1001 with pyrotinib, $n = 6$ per group) and ST-02-0103 **C** single-dose GQ1001 with pyrotinib, $n = 6$ per group) gastric cancers: GQ1001 combined with tucatinib or pyrotinib showed supra-additively enhanced anticancer effects. In the LD2-0017-201149 model, endpoint analysis showed that tumor size was smaller in the T-DXd group compared with the GQ1001-tucatinib combination group on Day 35, before which there was a cross between the tumor growth line of the T-DXd group and that of the GQ1001-tucatinib combination group; GQ1001 combined with pyrotinib showed an anticancer efficacy similar to T-DXd. Excitingly, combination of GQ1001 with pyrotinib caused complete response (CR) in all animals of the LD2-0017-201149 model; BR050 (HER2 + ++) breast infiltrating ductal carcinoma (**D** single-dose GQ1001 with tucatinib, $n = 5$ per group; **E** 2-cycle GQ1001 (Q3W × 2 doses) with pyrotinib, $n = 5$ per group; **F** 2-cycle GQ1001 (Q3W × 2 doses) with neratinib, $n = 5$ per group): Single- or repeated-dose GQ1001 combined with tucatinib, pyrotinib, or neratinib also demonstrated supra-additive anticancer activity, similar to T-DXd. **A**, **B** were from the same experiment, and **E**, **F** from the same experiment; for better clarify, they are shown separately. Datapoints represent group mean, and error bars represent standard deviation. Statistical tests used and exact p-values are provided in Supplementary Tables 17–20, on the figures themselves, and/or in the Source Data file. Source data are provided as a Source Data file.

Discussion

ADCs have significantly advanced targeted therapeutic efficacy for certain tumor types[38]. Several structurally-similar ADCs of GQ1001 and GQ1005 including T-DM1 and T-DXd[29] have been approved for patients with HER2-positive cancers; however, off-target toxicity and random conjugation-induced heterogeneity remain major concerns. Also due to treatment resistance, anti-HER2 therapies with enhanced safety and homogeneity remain an unmet clinical need.

GQ1001 and GQ1005 were developed by integrating the site-specific LDC conjugation platform based on enzyme immobilization technology with a unique stable ring-opening linker design, which confers ADC with high homogeneity and quality as well as enhanced stability in circulation via a concise process. Unlike most thiosuccinimide structure-based ADCs which are usually prone to retro-Michael or sulfhydryl exchange reaction leading to premature drug release in circulation and associated toxicities, our stable ring-opening linker prevents the undesired reactions, and further increases the hydrophilicity of the conjugate, due to the additional carboxylic group generated via ring-opening of thiosuccinimide prior to conjugation. Furthermore, the enzyme immobilization technology could facilitate recovery of products with greater purity and without redundant downstream or purification processes for the ADC preparation. GQ1001 and GQ1005 were highly-stable in plasma, and demonstrated favorable pharmacokinetics profiles and inspiring safety profiles and tolerability in various species including mice, rats, and monkeys.

The small-molecule DM1 is highly-cytotoxic and induces cell-death by inhibiting tubulin-polymerization[39]. Retro-Michael-addition probably occurs to T-DM1 linker (MCC) during incubation within cells or in circulation[40], releasing enough DM1 to cause cytotoxicity to normal cells. The linker of GQ1001 (MCC') with opened MCC structure was designed to avoid or markedly reduce retro-Michael reaction. This design dramatically reduces the extracellular drop-off of free DM1 prior to internalization, and avoids HER2-independent nonspecific effects and off-target cytotoxicity as seen for T-DM1[40]. As expected, GQ1001 demonstrated high cytotoxicity against HER2-positive cancer cells, but not against HER2-negative cancer cells or normal cells as opposed to T-DM1. This confirms the HER2-specific cytotoxicity of GQ1001, which is attributed to its highly-stable linker. These all support that GQ1001 is much safer than T-DM1.

P31-DM1 had no effect on HER2-negative MDA-MB-468 cells but DM1 and T-DM1 had a strong effect. The ring-opening linker P31 is highly hydrophilic and stably linked to the toxin DM1, making the linker-payload P31-DM1 hardly able to enter cancer cells or release free toxin DM1 to exert cytotoxicity. The small-molecule DM1 can relatively freely diffuse into cancer cells to exert cytotoxicity due to high hydrophobicity, irrespective of HER2 expression. T-DM1 with less stable linker always prematurely releases the toxin DM1 before binding HER2; the released DM1 could diffuse into and kill cancer cells, as well as normal cells (inducing off-target toxicity). This contrasts with the strict HER2 expression-dependent effect of GQ1001, which has significantly less off-target toxicity.

GQ1001 demonstrated great stability in circulation. In plasma, DM1-shedding of GQ1001 was only about 1/100 of that of T-DM1. In monkeys, DM1 could only be detected within 1 h after a single-dose administration of GQ1001 and 4 h after repeated-dose administration; while DM1 continuously fell off T-DM1, and could be detected 7 days after administration[12]. At 30 mg/kg in cynomolgus-monkeys, the C_{max} for DM1 from GQ1001 and T-DM1 was 0.72 and 63.90 ng/mL, respectively, and the AUCs were 0.0011 and 59.4 day*ng/mL, respectively. The blood exposure of DM1 for GQ1001 was significantly lower than that for T-DM1 as reported[41], and the HNSTD was markedly higher for GQ1001, indicating a wider therapeutic-window and most likely lower incidence of adverse events in humans possibly caused by free DM1 for GQ1001.

GQ1001 was well-tolerated in all toxicology studies of multiple species. Toxicities of T-DM1 in cynomolgus-monkeys mainly occur in liver, bone-marrow hematopoietic system, lymphatic system, nervous system, and epithelial-tissue[12]. Toxicity spectrum of GQ1001 was narrow and significantly milder than that of T-DM1. Particularly, nervous system toxicity can be induced by high-level free-DM1 released from T-DM1, while it was not observed in any of the GQ1001 toxicity studies. All the abnormalities noted in preclinical safety studies of GQ1001 were fully-recovered or towards recovery at the end of recovery-period, indicating the reversible and manageable nature of the adverse-events. Few of the preclinical safety findings were considered to have toxicologic significance due to small magnitude, within/close to the range of background-values, and/or without related histopathologic alterations. HNSTD of GQ1001 in cynomolgus-monkeys was as high as 45 mg/kg; contrastively, HNSTD of T-DM1 was limited to 10 mg/kg due to irreversible peripheral-neuropathy.

In the clinical setting, major adverse events of T-DM1 include thrombocytopenia, which limits the maximum tolerated dose (MTD) to 3.6 mg/kg every 3 weeks, and peripheral neuropathy as typical toxicity of tubulin-inhibitor-conjugated ADCs[8,10–12,29,42]. With low exposure of DM1, for GQ1001 no peripheral neuropathy was noted in all the preclinical safety studies or the phase-I trial. MTD of GQ1001 in humans was not reached with dose up to 8.4 mg/kg without any dose-limiting toxicities (DLTs) noted, and the suggested safety is superior to T-DM1 and comparable with trastuzumab, with the highest recommended loading-dose being 8.0 mg/kg. GQ1001 induced no common eye or liver injury associated with traditional ADCs or lung toxicities in monkeys or patients so far. Compared to T-DM1, GQ1001 demonstrated superior safety-profile and acceptable and favorable tolerability, possibly partly due to superior homogeneity and stability.

GQ1001 significantly inhibited HER2-positive tumor xenografts not well-responsive to trastuzumab[43]. Overall, efficacy of GQ1001 was mostly noninferior to that of T-DM1. For HER2-positive cancers, lower-DAR ADC could already deliver sufficient payloads inducing cytotoxicity[10]. Higher-DAR does not necessarily improve anticancer-

https://doi.org/10.1038/s41467-025-64675-6

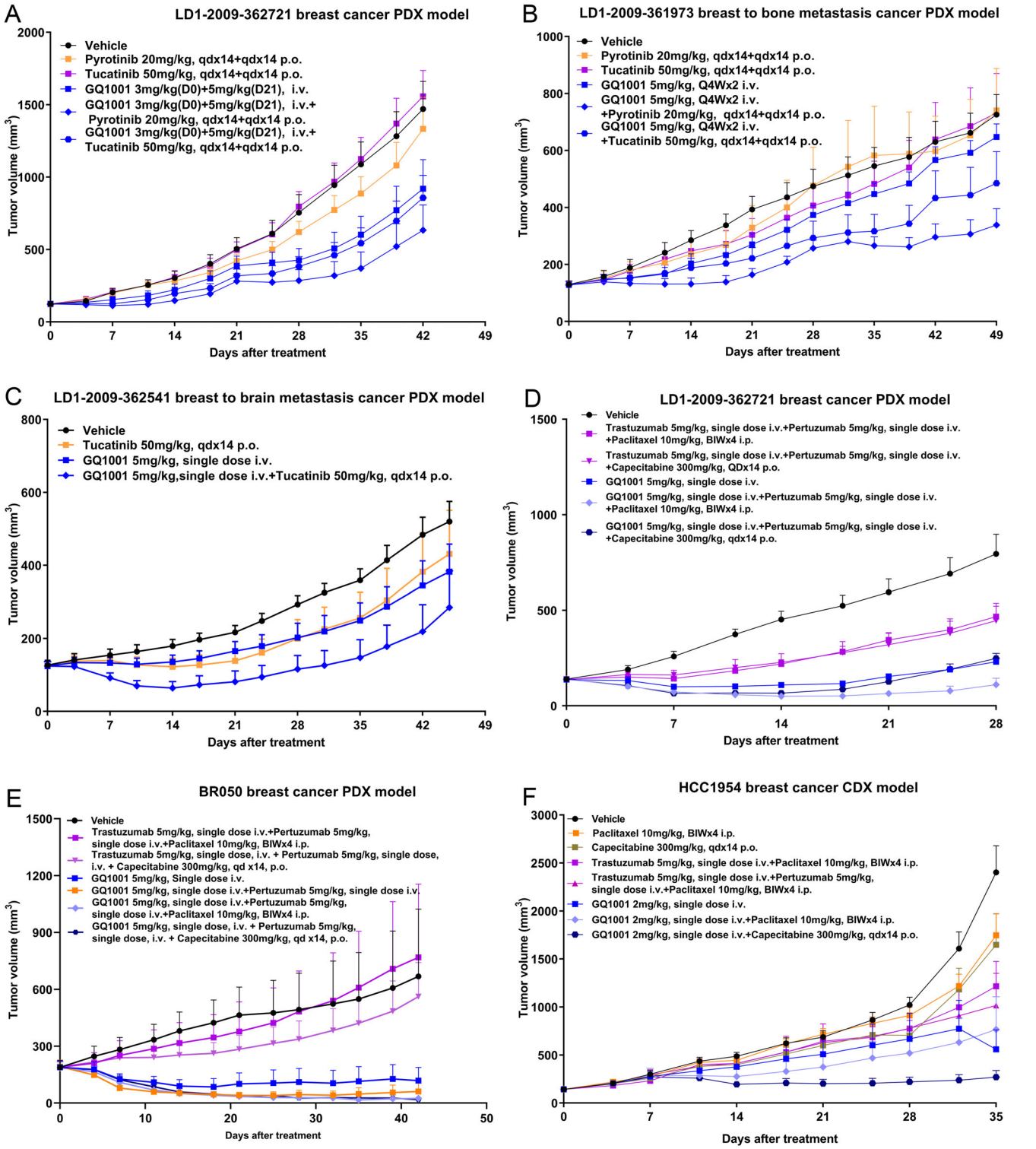

efficacy, possibly due to instability and faster clearance of ADC, and may increase toxicity[5]. Also, due to the substantially improved linker stability, GQ1001, although with a lower DAR, could more efficiently and specifically deliver the toxin drug DM1 into target cancer cells to exert more targeted and specific anticancer effects, without significant premature release of payloads or linker-payloads before entering cancer cells, which also reduces off-target toxicities. Linker-stability correlates positively with in vivo ADC efficacies[37]. Notably, GQ1001 remained active in heavily-pretreated trastuzumab-refractory HER2-amplified cancer xenograft models.

GQ1001 also showed efficacy in cancers resistant to T-DXd due to high ABCG2 expression, potentially offering an alternative treatment option for such cancers. DXd is a substrate of ABCG2 (BCRP) and ABCB1 (MDR1, P-gp)[27,28], while DM1 and the main metabolites of GQ1001, K'-MCC'-DM1, are not major ABCG2 substrates. DM1 efflux depends on ABCB1, ABCC1 (MRP1), and ABCC2 (MRP2), but not on ABCG2[26]. Positive expression of ABCG2, a key protein mediating T-DXd treatment resistance[27,28], is prevalent across breast cancer (irrespective of HER2 expression), non-small cell lung cancer, and gastric cancer (Supplementary Tables 29-30), which are major indication cancers for

Fig. 7 | In vivo efficacies of GQ1001 combined with HER2-targeting tyrosine kinase inhibitors (TKIs), and with chemotherapy and/or HER2-targeting monoclonal antibody in multiple primary or metastatic cancers. A–C Tumor growth curves (tumor sizes over time) showing in vivo anticancer efficacies of GQ1001 in combination with TKIs and other groups in patient-derived xenograft (PDX) mouse models: HER2-positive LD1-2009-362721 (**A** GQ1001 (Q3W × 2 doses) with tucatinib or pyrotinib, $n = 6$ per group) and LD1-2009-361973 bone-metastatic (**B** GQ1001 (Q4W × 2 doses) with tucatinib or pyrotinib, $n = 6$ per group) breast cancer; and LD1-2009-362541 (**C** single-dose GQ1001 with tucatinib, $n = 6$ per group) brain-metastatic breast cancer. In cases with breast cancer resistant to pyrotinib (LD1-2009-362721 PDX model) and those with heavy tumor metastasis burden (LD1-2009-361973, bone metastasis; LD1-2009-362541, brain metastasis), combo treatment of GQ1001 with tucatinib or pyrotinib still exhibited good supra-additive antitumor activity. **D–F** Tumor growth curves showing the anticancer efficacies of GQ1001 in combination with chemotherapy and/or pertuzumab and other groups in human breast cancer LD1-2009-362721 (**D** single-dose GQ1001 with pertuzumab and paclitaxel/capecitabine, $n = 6$ per group) and BR050 (**E** single-dose GQ1001 with pertuzumab and paclitaxel/capecitabine, $n = 6$ per group) PDX models, and HCC1954 cell-derived xenograft (CDX) model (**F** $n = 6$ per group). In addition to the supra-additive effects when in combination with TKIs, GQ1001 has also demonstrated good improved antitumor effects when used with chemotherapeutic agents and/or HER2-targeting monoclonal antibodies. In the LD1-2009-362721 and BR050 breast cancer PDX model, GQ1001 combined with pertuzumab and chemotherapy (paclitaxel or capecitabine) showed better antitumor activity than triple combination treatment with trastuzumab, pertuzumab, and chemotherapy (TPH), the current standard first-line regimen for HER2-positive breast cancer. Furthermore, GQ1001 combined with chemotherapy also had better efficacy than TPH treatment in the HCC1954 CDX model. Datapoints represent group mean, and error bars represent standard deviation. Statistical tests used and exact p-values are provided in Supplementary Tables 21–26, on the figures themselves, and/or in the Source Data file. Source data are provided as a Source Data file.

T-DXd. DM1 efflux could also be influenced by the linker, which is stable in GQ1001.

ADCs are mainly approved as single-agents. Our animal-model studies could provide important clues for clinical development of effective ADC-based combination-treatment strategies. In gastric-cancer and breast-cancer PDX-models, GQ1001 combo-therapy with HER2-targeting TKIs (tucatinib, pyrotinib, or neratinib) showed strong supra-additively enhanced anticancer-effects, some of which were similar to T-DXd. Combo-treatment of GQ1001 with TKIs also supra-additively inhibited tumor-growth in TKI-resistant PDX-models and metastatic breast-cancer PDX-models. These suggested that GQ1001 combined with TKIs could bring supra-additively enhanced treatment-effects to patients especially those with strongly-heterogeneous, drug-resistant, and/or metastatic cancers[44,45]. Moreover, GQ1001 combo-therapy with chemotherapeutics (paclitaxel or capecitabine) demonstrated obviously better efficacy than TPH-therapy (first-choice treatment for HER2-positive breast-cancer) in xenograft models, which would provide a promising treatment choice. Co-administration of antibody may improve the cancer penetration, intra-tumoral distribution, and single-cell targeting of ADCs, enhancing anticancer efficacy and host survival[46,47].

GQ1005 was modified from T-DXd in a way similar to GQ1001 from T-DM1. Both GQ1001 and GQ1005 are developed based on the stable ring-opening linker and irreversible LDC conjugation technology, and show strong stability, minimal payload/linker-payload release in circulation, and low toxicity. When dosed at or near the MTD, ADC can demonstrate enhanced efficacy[48], suggesting room for improvement in efficacy through improving safety. Despite lower DAR, GQ1005 demonstrated only slightly weaker in vitro cytotoxicity compared to T-DXd, whose DAR nearly halved within 4 days, in HER2-amplified cancer cells. GQ1005 showed stronger ADCC activity, superior stability, and a higher tumor-to-plasma payload exposure ratio compared to T-DXd. In CDX and PDX models, GQ1005 demonstrated robust dose-dependent anticancer efficacies mostly comparable to T-DXd across various cancers. In cynomolgus monkeys, GQ1005 demonstrated minimal payload DXd shedding in circulation, with HNSTD being twice that of T-DXd, and with no mortality or lung toxicity observed, suggesting better safety than T-DXd. GQ1001 and GQ1005 have the potential to be used as super Herceptin with preeminent stability and safety and satisfactory efficacy.

The essence of our work is to importantly highlight that the innovative application of the proprietary one-enzyme, one-step site-specific ligase-dependent conjugation (LDC) technology and the uniquely-designed stable thiosuccinimide ring-opening linker for anticancer ADCs could significantly enhance stability and safety and meaningfully reduce off-target toxicities in ADCs, major and prominent challenges faced by the ADC world currently, whilst the modification does not significantly impact efficacy. Recently it was suggested that compared to chemotherapeutic drugs (small-molecule payload cytotoxins), ADC did not significantly expand the therapeutic window for cancer (but only shifted it), which is in urgent need of revision[48]. In this work, we demonstrate that: Through innovative application of the promising LDC conjugation technology and the stable ring-opening linker technology, a meaningfully widened therapeutic window is steadily achievable; moreover, taking advantage of this significant safety and stability improvement, ADC-based therapies with multiple combination choices and against multiple refractory cancers become more viable.

This study has some limitations. The LD1-0006-217643 model was the only PDX model with available specimens preserved for endpoint histopathology analysis. At the endpoint (Day 60) of the LD1-0006-217643 PDX experiment, while tumor volume was significantly smaller and tumor weight was significantly lower in the GQ1001-treated groups (Fig. 4E & Supplementary Table 13), there were no significant differences in the expressions of HER2, the apoptosis marker cleaved Caspase-3, or the proliferation marker Ki-67 in the existing or remaining tumor tissue between the 10 mg/kg GQ1001 group and the vehicle control group using immunohistochemistry staining (Supplementary Fig. 10). This might be partly due to that many of the cancer cells sensitive to GQ1001 were eliminated at the endpoint, leaving the insensitive ones (with resistance due to other mechanisms than HER2 expression) behind. On the sampling day (Day 60; 30 days away from the last drug administration), the drug exposure concentration within tumors was already low with weak pharmacological effect, and the relevant mechanisms were already hardly observable. Also, the findings might be biased by the small number of available analyzable specimens. Histopathology examinations of tumor xenografts at the endpoint of PDX experiments using drug combinations were not done. Drug combinations typically had stronger efficacies than single agents, with residual diseases mostly small and not applicable for meaningful histopathology analyses, and we did not have sufficient specimens for such analyses. In the CDX/PDX experiments, tumor growth curves indicative of drug efficacy were majorly focused on. Decreased proliferation and increased apoptosis induced by the investigated ADC in line with the antitumor activity has been shown using multiple cell models (e.g., Fig. 3 and S2). It is important to further improve the molecular validation of activity in future studies, by including in vivo experiments with animal models sacrificed at early timepoints (e.g., within a week of starting treatment), to show loss of HER2 expression (on-target effect of ADC), and evidence of decreased proliferation and increased apoptosis in line with anti-tumor activity. There were some PDX models (ST-02-0318, CTG-0927, and LD1-0006-217643) where comparisons of GQ1001 with T-DM1 or T-DXd were not made, and they were merely designed to show the dose-dependent anticancer efficacies of GQ1001 monotherapy, with the inter-drug comparisons shown in other models.

https://doi.org/10.1038/s41467-025-64675-6

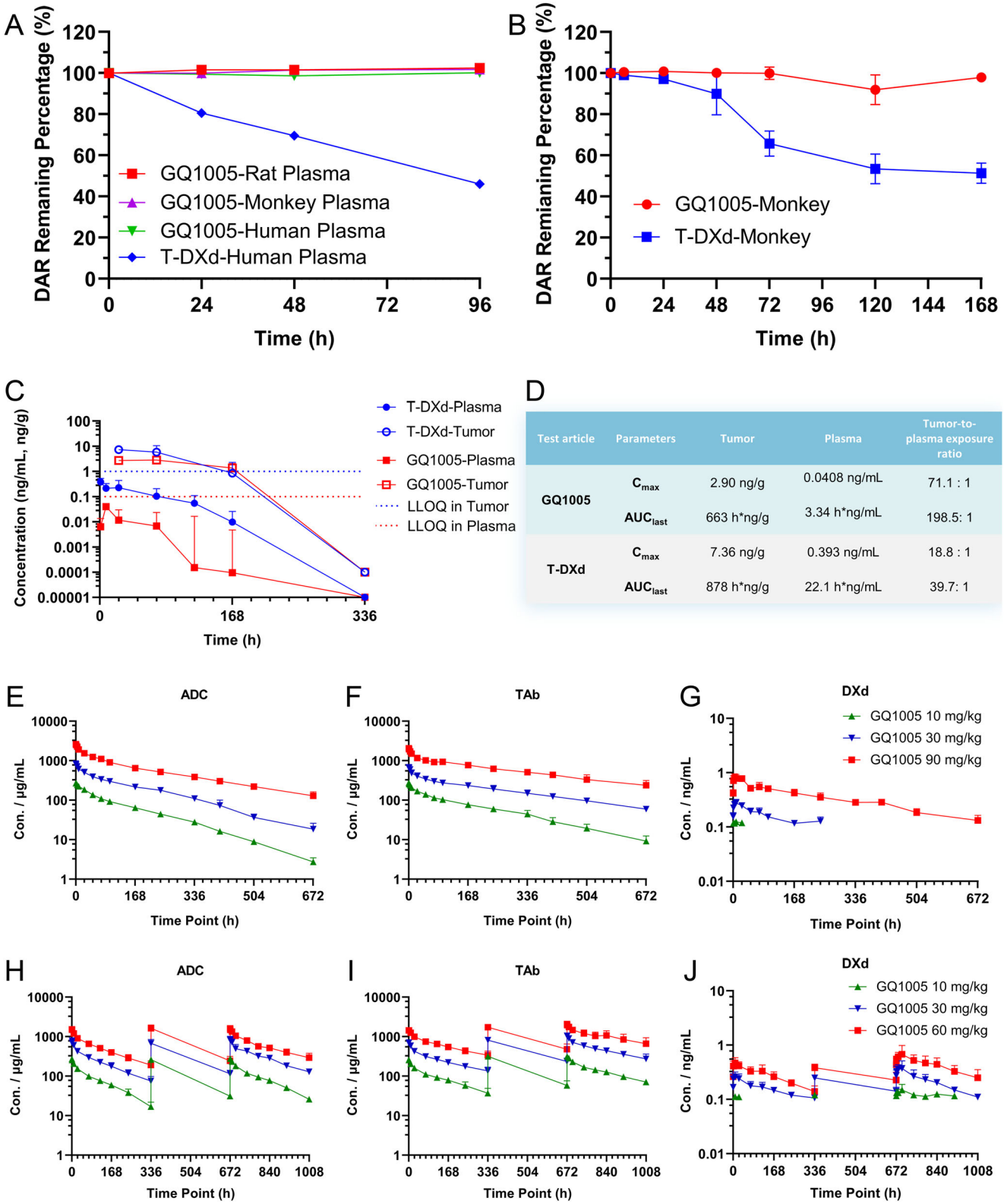

Test article	Parameters	Tumor	Plasma	Tumor-to-plasma exposure ratio
GQ1005	C_{max}	2.90 ng/g	0.0408 ng/mL	71.1 : 1
	AUC_{last}	663 h*ng/g	3.34 h*ng/mL	198.5: 1
T-DXd	C_{max}	7.36 ng/g	0.393 ng/mL	18.8 : 1
	AUC_{last}	878 h*ng/g	22.1 h*ng/mL	39.7: 1

Conclusively, the application of the LDC technology and ring-opening linker improves stability, safety, and pharmacokinetics profiles and reduces off-target toxicity in developing some anticancer ADCs (e.g., GQ1001 and GQ1005) compared to similar ADCs, with mostly similar and noninferior efficacies. GQ1001 and GQ1005 demonstrate unweakened in vivo inhibitory efficacies against various HER2-overexpressing cancer types, including those heavily-pretreated by multiple HER2-targeting drugs, with enhanced safety. Anticancer efficacy of GQ1001 with high homogeneity is supra-additively enhanced by HER2-targeting TKIs and/or chemotherapeutic agents. GQ1001 shows efficacy in cancers resistant to T-DXd due to high ABCG2 expression. GQ1001 and GQ1005, used alone or in combination, are thus attractive and promising ADCs to treat refractory HER2-amplified cancers with reduced toxicity.

Fig. 8 | Stability and pharmacokinetic/toxicokinetic data of GQ1005. A, **B** Dynamic changes of the drug-to-antibody ratios (DAR) of GQ1005 and T-DXd (**A**) ex vivo in plasma and (**B**) in vivo in circulation in cynomolgus monkeys ($n = 3$ per group). GQ1005 demonstrated good stability both ex vivo and in vivo when compared to T-DXd, whose DAR nearly halved within 4 days in plasma and 5 days in circulation, respectively. **C**, **D** Payload enrichment in tumor and plasma of NCI-N87 human gastric cancer-bearing BALB/c nude mice for GQ1005 versus T-DXd ($n = 3$ per group). Despite lower DAR, GQ1005 demonstrated high payload enrichment in tumor, comparable to T-DXd, but had markedly lower payload exposure in plasma than T-DXd (AUC, 3.34 vs 22.1 h*ng/mL). The tumor-to-plasma payload exposure ratio for GQ1005 with enhanced linker stability was markedly higher than that for T-DXd (AUC, 198.5:1 vs 39.7:1). **E**–**G** Pharmacokinetic/toxicokinetic studies of single-dose intravenous GQ1005 infusion in cynomolgus monkeys ($n = 6$ per group). The mean serum DXd concentration was far lower than the mean serum GQ1005 ADC concentration. The serum DXd concentration in the 10 mg/kg group measured slightly higher than the lower limit of quantification (LLOQ) or was even unmeasurable. In the 30 and 90 mg/kg GQ1005 groups, the mean C_{max} and $AUC_{0\text{-}t}$ for DXd remained low. **H**–**J** Pharmacokinetic study of repeated-dose intravenous GQ1005 administration in cynomolgus monkeys ($n = 10$ per group). The exposure level ($AUC_{0\text{-}t}$) of GQ1005 ADC after repeated administration was similar to that after the first administration, indicating no drug accumulation. After repeated administration, the half-life $t_{1/2}$ of GQ1005 ADC (4.04-6.65 days) and TAb (6.59-10.20 days) was comparable to that after the first administration. After the first and last administration, DXd was only detectable at certain timepoints in the 10 mg/kg GQ1005 group. With increasing dose, the timepoints where DXd was detectable gradually increased in the 30 and 60 mg/kg groups, with DXd concentrations slightly higher than the LLOQ. The average C_{max} and $AUC_{0\text{-}t}$ of DXd increased with increasing dose of GQ1005 (30-60 mg/kg). In Figs. 8B, 8C & 8E–J, data are presented as mean values with standard deviations. Source data are provided as a Source Data file.

Methods

Materials

Trastuzumab (lot. No., N7124) and T-DM1 (lot. No., N5004B01) were commercial products from Roche (Mannheim, Germany). DM1 (lot. No., MTB-20180717-02) was purchased from Brightgene (Suzhou, China), and T-DXd (lot. No., 1330814) from Daiichi Sankyo (Tokyo, Japan). For TKIs, tucatinib (lot. 20092703) was from Famo biotechnology (Shanghai, China), pyrotinib (cat. CR3773) from Taizhou Crene Biotechnology (Taizhou, China), and neratinib (lot. 20062803) from Jinan Sanzhi Medical (Jinan, China). Pertuzumab (lot. H0465B01) was from Roche Pharma (Schweiz) AG (Basel, Switzerland), paclitaxel (lot. H026876AB) from Hosipira Australia (Springvale, Australia), and capecitabine (lot. C12685939) from Shanghai Macklin Biochemical (Shanghai, China).

Generation of GQ1001 and GQ1005

mAb production. The mAb of GQ1001 and GQ1005 was designed with a ligase recognition motif LPXTGG inserted at the C-terminus of the light chain of trastuzumab antibody, and the mAb was produced in CHO-K1 cell-line.

Linker-payload production. The linker-payload of GQ1001 (P31-DM1-α isomer) was synthesized via two chemical steps: 1) Maleimide on P31 reacted with DM1 sulfhydryl to form a thiosuccinimide with two chiral centers; 2) Ring-opening hydrolysis generated two positional isomers (α and β) per sulfur distance from amide bond, which were purified by liquid-phase prep to remove impurities and contents of β-isomer.

The linker-payload of GQ1005 (OL11119) was synthesized using MC-GGFG-DXd and a branch peptide linker containing two cysteines via two chemical steps: 1) The maleimide on MC-GGFG-DXd reacted with the sulfhydryl group on the cysteine of the linker to form a thiosuccinimide; 2) The linker-payload was generated via ring-opening hydrolysis of the thiosuccinimide followed by purification using liquid-phase prep.

Further information and the characterization data are detailed in Supplementary Note 5 and Supplementary Figs. 11-16.

Enzyme-immobilizing resin and conjugation column production. The engineered Sortase A was expressed by a microbial system and the highly active enzyme was purified by multi-step ion and hydrophobic chromatography. The engineered Sortase A and agarose resin were mixed at room temperature for immobilization. Subsequently, the agarose resin was washed with sodium hydroxide and a high-salt buffer to remove impurities. The immobilized enzyme-resin could be pre-packed into columns with different specifications according to requirements.

GQ1001 and GQ1005 production. The conjugation process did not require the addition of organic phase. The ADC was manufactured using GeneQuantum's proprietary enzymatic site-specific conjugation technology known as ligase-dependent conjugation (LDC). The conjugation process occurred within a single-use column pre-packed with the immobilized ligase resin. The mAb and linker-payload solutions were passed through the conjugation column, with a residence time of ~20 min for conjugation. The resulting conjugation solution was purified by affinity chromatography using MabSelect Sure LX Resin, followed by anion exchange chromatography (AEX) using Q SepharoseTM Fast Flow Resin (GE Healthcare) and cation exchange chromatography (CEX) using CaptoTM MMC ImpRes Resin (GE Healthcare). The GQ1001/GQ1005 was buffer-exchanged to a storage formulation buffer through ultrafiltration/diafiltration (UF/DF) and stored at -40 °C. The drug-antibody ratio (DAR) value of GQ1001/GQ1005 was analyzed by Hydrophobic Interaction Chromatography (HIC)-High-Performance Liquid Chromatography (HPLC) analysis.

HER2-binding activity assay

The in vitro binding affinities of GQ1001/GQ1005, GQ1001/GQ1005 mAb, trastuzumab, and T-DM1 to HER2 ECD were detected using enzyme-linked immunosorbnent assay (ELISA), and relative affinities were calculated with trastuzumab as positive control. The binding affinity and kinetics of GQ1001 (0.2 μg/mL) to recombinant human HER2 protein (3.125-100 nM), FcRn and Fcγ receptors and the binding kinetics of GQ1001 to HER2 across species were determined using SPR. Kinetic association (Ka), kinetic dissociation (Kd), and kinetic equilibrium dissociation constants (KD) were analyzed using Biacore T200 software v3.0.

Ex vivo stability in plasma

Samples were prepared by spiking GQ1001/GQ1005, T-DM1, or T-DXd stock solution into pooled plasma of each species (SD rat, cynomolgus monkey, and human) and the GQ1001 formulation buffer, respectively, at the nominal concentration of 1 mg/mL, and then incubated at 37 °C. All samples were stored in a freezer with light protection at ≤-65 °C upon reception until analysis. Free DM1 or DXd was detected using the LC-MS/MS method at different timepoints, respectively, with shedding ratio further calculated. DAR was detected using the high-resolution LC-MS method.

Cell lines, cell culture, and reagents

The human breast cancer cell lines (HCC1954, cat. CRL-2338; SK-BR-3, cat. HTB-30; BT474, cat. HTB-20; and MDA-MB-468, cat. HTB-132), human gastric cancer cell line NCI-N87 (cat. CRL-5822), and human ovarian cancer cell line SK-OV-3 (cat. HTB-77) were purchased from ATCC. HCC1954 and NCI-N87 cells were cultured in 90% RPMI-1640 medium with 10% FBS, SK-BR-3 and SK-OV-3 cells in 90% McCoy's 5 A plus 10% FBS, BT474 cells in 90% Hybri-care plus 10% FBS, and MDA-MB-468 cells in 90% L-15 added with 10% FBS. CellTiter-Glo® (CTG) Luminescent Kit and Caspase-Glo™ 3/7 Assay Kit were purchased from

Promega (cat. No., G7573/ G8091, WI, USA), Cell Cycle Analysis Kit was bought from Fusion-Biotech (cat. No., FS9527, Shanghai, China), and LDH detection kit was from Roche (cat. No., 04744926001, Mannheim, Germany). The manufacturer of propidium iodide (PI) was Invitrogen. Human serum was from Zenbio, and the SPR reagents from GE Healthcare (Massachusetts, USA).

Internalization into tumor cells

HER2-positive HCC1954 (for GQ1001) and NCI-N87 and BT474 (for GQ1005) cells were cultured until nearly confluent, harvested, and re-suspended in cold binding buffer (DPBS + 2% FBS). GQ1001/GQ1005, GQ1005 mAb, or T-DM1 sample was co-incubated with AF647-labeled anti-human lgG Fc antibody and then added to the cells with a final sample concentration of 6.67 nM for 1 h. Then cells were washed and re-suspended in binding buffer, followed by incubation at 37 °C for 10, 30, 60, 90, 120, 150, 180, 210, and/or 240 min, respectively. Internalization was stopped by placing the cells on ice. Then cells were quenched, washed twice, and assayed using flow cytometry, with data analyzed using the FlowJo software. Internalization ratio (Y_t) was calculated.

Cytotoxicity assay

The cytotoxicity of GQ1001 and other articles was investigated in various cell lines (HCC1954, SK-BR-3, BT474, MDA-MB-468, NCI-N87, SK-OV-3, H2110, and CFPAC-1). Tumor cells in good growth condition with a cell fusion degree of about 80% were digested by 0.25% trypsin, collected, placed in 96-well plates, and cultured overnight. After cell adherence, drug was administered at multiple concentrations. After 72-h incubation at 37 °C, CellTiter-Glo® luminescent kits were used to detect cell viability, which was calculated as: $(RLU_X - RLU_{Puro}) / (RLU_{Control} - RLU_{Puro}) \times 100\%$.

Cell cycle and apoptosis assays

HER2-positive (HCC1954, NCI-N87, and SK-BR-3) or HER2-negative (MDA-MB-468 and HepG2) tumor cells were cocultured with the test article GQ1001/GQ1005, GQ1005 mAb, T-DXd, T-DM1, or DM1, respectively. After incubation for 24 h, the harvested cells were stained by propidium iodide, and then cell cycle was evaluated using flow cytometry. For apoptosis assay, 48 h after treatment, Caspase-Glo® 3/7 assay kit was used for detection[37].

ADCC assay

HER2-positive BT474 or SK-BR-3 cells were co-cultured with human PBMCs with an effector-target (E-T) ratio of 20:1. Cells were then treated with GQ1001, GQ1005, or other test articles for 4 h. Then medium supernatant was transferred to a tissue-culture (TC)-treated clear flat-bottom 96-well microplate for lactate dehydrogenase (LDH) detection. The OD data from microplate reader were incorporated into the formula below, and the result was analyzed using log (agonist) vs response – variable slop (four parameters) function with GraphPad Prism. Lysis ratio (L) = $[OD_{E+T+Ab} - OD_{E+T} - OD_{T+D} + OD_T] / [OD_{T+Lysis} - OD_T] \times 100\%$, where E + T + Ab was for antibody treatment, E + T for control of PBMC, T + D for control of antibody, T for experimental background, and T + Lysis for control of the strongest signal.

Identification of catabolites of GQ1001 in HER2-positive BT474 cells

To investigate whether catabolites of GQ1001 in HER2-positive cells included K′-MCC′-DM1 and MCC′-DM1, HER2-positive human breast cancer BT474 cells were treated with GQ1001 for 24 h, and then the medium supernatant and cells were collected. Cells were lysed by 100 µL cell-lysis buffer (50 mM Tris-HCl, 100 mM NaCl, 0.1% Triton X-100) and centrifuged at 4 °C, 17,000 g for 10 min. Then all the supernatant was pipetted into another tube, added with 400 µL MeOH, whirled, and placed at -25 °C for 120 min. 100 µL medium supernatant was also pipetted and added with 400 µL MeOH, whirled, and placed at -25 °C for 120 min. The above samples were whirled and centrifuged at 4 °C, 12,000 g for 5 min. The supernatant was transferred to new tubes, volatilized under nitrogen, and then added with 100 µL MeOH to dissolve again. The solution was centrifuged at 4 °C 12,000 g for 5 min, and analyzed using AB Sciex QTRAP 5500 with the following settings: Injection volume: 20 µL; Ion source: ESI; Ionization model: Positive; Multiple reaction monitoring: K-MCC-DM1: m/z 1103.6 → 485.3; MCC-DM1: m/z 957.7 → 485.3; K′-MCC′-DM1: m/z 1120.6 → 1058.5; MCC′-DM1: m/z 1010.3 → 975.2.

Catabolites of GQ1001 in HER2-positive BT474 cells at different timepoints

To investigate whether catabolites of GQ1001 in HER2-positive cells included DM1, HER2-positive human breast cancer BT474 cells were treated with 0.30 mg/mL GQ1001 sample for 4, 8, 24, 48, and 72 h, and then the medium supernatant and cells were collected. Then the concentrations of DM1 in cell medium supernatant and cell lysate were analyzed. Cells were lysed by 150 µL cell-lysis buffer (50 mM Tris-HCl, 100 mM NaCl, 0.1% Triton X-100) and centrifuged at 4 °C, 17,000 g for 10 min; then the supernatant was collected. 40 µL medium supernatant and cell lysate were pipetted into the plate, added with 20 µL 30 mM TCEP and 5 mM NH_4OAc in water, whirled at room temperature for 10 min, and centrifuged at 4 °C, 3176 g for 10 min. 100 µL supernatant was pipetted into a new 1-mL 96-well plate and used for DM1 analysis using Shimadzu LCMS-8050 with the following settings: Injection volume: 20 µL; Ion source: ESI; Ionization model: Positive; Multiple reaction monitoring: DM1: m/z 738.4 → 547.2. The lower limit of the DM1 quantitative analysis method was 0.5 ng/mL.

In vivo antitumor activity studies

CDX or PDX tumor models were constructed by engrafting human cancer cells-derived or patient cancer tissue-derived xenografts into female nude BALB/c mice (for CDX models) or NU/NU, NCG, or NOD SCID mice (for PDX models), and were then treated with GQ1001, GQ1005, or others. Information on CDX and PDX models is listed in Supplementary Table 32. Mice received tumor xenografts through subcutaneous inoculation at the right flank (5 or 10 $\times 10^6$ cells/mouse in 0.2 mL of PBS with Matrigel (1:1)), and were randomly assigned mostly when tumors reached an average size of 150-200 mm^3, with treatments then initiated. Tumor sizes were recorded twice a week after administration, and tumor weights were measured at study termination.

Tumor payload enrichment study

HER2-positive NCI-N87 human gastric cancer-bearing BALB/c nude mice were administered intravenously a single dose of GQ1005 or T-DXd (10 mg/kg). Tumor and plasma samples were collected up to 336 h post dose, and concentrations of free payload (DXd) in tumor and plasma were determined using LC-MS/MS.

Pharmacokinetics and toxicity studies

Single-dose pharmacokinetics studies of GQ1001 (6, 20, 60, and 90 mg/kg) and GQ1005 (10, 30, and 90 mg/kg) were conducted in SD rats and cynomolgus monkeys, respectively. The pharmacokinetics of GQ1001/GQ1005 ADC, GQ1001/GQ1005 TAb, and DM1/DXd were characterized following a single intravenous infusion of GQ1001/GQ1005. Blood samples were collected at pre-dose, 5 minutes, and 1, 4, 8, 24, 48, 72, 96, 168, 336, 408, 504, and/or 672 h. The concentrations of GQ1001/GQ1005 and GQ1001/GQ1005 TAb in samples were determined using ELISA, and the concentration of DM1/DXd was determined using LC-MS/MS. Pharmacokinetics parameters assessed included T_{max}, C_{max}, AUC_{0-t}, MRT, $T_{1/2}$, and V_d.

GLP-compliant, pivotal, repeated-dose (7-week for GQ1001, and 4-week for GQ1005) toxicology studies were conducted in cynomolgus monkeys. 40 cynomolgus monkeys (5/sex/group) were randomly

assigned and administered with the test article (GQ1001: 10, 30, and 45 mg/kg; or GQ1005: 10, 30, and 60 mg/kg) or vehicle, for 3 times (once every 3 weeks for GQ1001, and once every 2 weeks for GQ1005) in a dosing phase (7-week for GQ1001, and 4-week for GQ1005). At the end of the dosing phase, 3 animals/sex/group were necropsied, and the remaining 2 animals/sex/group were necropsied after a recovery phase (6-week for GQ1001, and 4-week for GQ1005). The following parameters were assessed: Clinical observations (including functional assessment of central nervous system), body weight, food consumption, ophthalmology, body temperature (rectal and surface), local irritation, cardiovascular and respiratory system function (e.g., ECG and respiratory frequency), hematology, coagulation, plasma chemistry, urinalysis, immunophenotype, immunoglobulins, complements, gross pathology, organ weights, and microscopic histopathology, with toxicokinetic evaluations concurrently performed.

ICH M3 (R2), S6, and S9 guidelines, and 21 CFR 58 were followed, and same batch of GQ1001 drug substance (DS; Batch No.: A190401R) was used in all GLP toxicology studies.

Toxicokinetics and toxicities in rats

Single-dose GLP toxicology study of GQ1001 (20, 60, 120 mg/kg), P31-DM1/toxin-linker (4 mg/kg), and DM1 (0.2 mg/kg) in SD rats. DM1 and P31-DM1 were tested separately in SD rats in respect of the potential toxicity of the payload. The pharmacokinetics of GQ1001 ADC, GQ1001 total antibody (TAb), DM1, and K′-MCC′-DM1 were characterized following a single *i.v.* infusion of GQ1001, and the pharmacokinetics of GQ1001 monoclonal antibody (mAb) were characterized following a single *i.v.* infusion of GQ1001 mAb in SD rats. K′-MCC′-DM1 is an important metabolite of GQ1001. Therefore, the pharmacokinetics of K′-MCC′-DM1 and its possible further metabolite DM1 were evaluated after a single administration of K′-MCC′-DM1 in SD rats. Blood samples were collected at pre-dose (0 h), 5 min, 1 h, 4 h, 8 h, 24 h, 72 h, 168 h, 336 h, 504 h, and 672 h for GQ1001 and mAb groups, and at pre-dose (0 h), 5 min, 30 min, 1 h, 2 h, 4 h, 8 h, 24 h, 48 h, and 72 h for the K′-MCC′-DM1 group. Concentrations of GQ1001, GQ1001 TAb, and GQ1001 mAb in samples were determined using ELISA, and the concentration of K′-MCC′-DM1 was determined using HPLC-MS/MA. Pharmacokinetics parameters assessed included T_{max}, C_{max}, $AUC_{0\text{-}t}$, MRT, $T_{1/2}$, and Vd. Toxicity profile was concurrently evaluated regarding clinical observation, body weight, food consumption, and pharmacokinetics. Animals were sacrificed after the sample collection of the last time-point.

Toxicokinetics and toxicities in cynomolgus monkeys

The single-dose toxicokinetics profile of GQ1001 was characterized in a GLP-compliant study. 30 Cynomolgus monkeys were randomly assigned to 5 groups (3/sex/group) and administered 0 (vehicle), 10, 30, 45 mg/kg GQ1001 or 45 mg/kg GQ1001-mAb (antibody intermediate) by a single 20-min i.v. infusion. The observation period was 6 weeks.

The in vivo toxicokinetics and toxicity profiles of GQ1001 following repeated doses were characterized in a GLP-compliant, 7-week repeated-dose toxicity study of cynomolgus monkeys using the clinically-relevant route (*i.v.*) and schedule (*Q3W*×3 doses) of administration. Cardiovascular and respiratory system safety pharmacology, local irritation and toxicokinetics, and immunogenicity assessment with 6-week recovery were also evaluated in Cynomolgus monkeys. A total of 40 Cynomolgus monkeys were enrolled in the pre-dose and dosing phase and randomly assigned into 4 groups (5/gender/group), with 0 (vehicle), 10, 30, and 45 mg/kg of GQ1001 or T-DM1 administered intravenously for 7 weeks (once every 3 weeks for a total of 3 doses), respectively; 16 monkeys (2/gender/group) were enrolled in the 6-week recovery phase.

The main endpoints included: Death/dying, clinical observation, body weight, and food intake; clinical pathological examination included: Hematology, coagulation, serum biochemistry, and cardiotoxicity biomarker troponin I, accompanied by ECG. At the end of the administration period, gross anatomy and histopathological examination of main tissues/organs were performed.

Toxicities in mice

100 female ICR mice were randomly divided into 8 groups. Group 1 was injected with sodium chloride as negative control; Group 2 was given 90 mg/kg T-DM1; Groups 3-6 were given GQ1001 at doses of 90, 165, 240, and 300 mg/kg, respectively; Group 7 was given 300 mg/kg GQ1001 mAb as control; Group 8 was given 6.24 mg/kg P31-DM1 as control. The number of animals was 16 in Group 1, and 12 in Groups 2-8. All animals were injected once intravenously on Day 1 with a dosage volume of 20 mL/kg, and the injection was completed within 30 s. Animals in Group 1 were euthanized on Days 4, 7, 14, and 21, respectively, with 4 euthanized each time; Animals in Groups 2-7 were euthanized on Days 7, 14, and 21, with 4 euthanized each time; animals in Group 8 were euthanized on Days 4, 7, and 14, with 4 euthanized each time. Animals were observed clinically and pathologically, with body weight and food intake measured, and blood cell counts, blood biochemical indicators, and organ weight examined.

Single-dose toxicity in SD rats

A total of 120 rats (10 animals/gender/group) were given single intravenous infusion of vehicle (GQ1001 preparation buffer) at 0 mg/kg, GQ1001 at 20, 60, and 120 mg/kg, P31-DM1 at 4 mg/kg (linker-toxin, equal to 257.92 mg/kg GQ1001), and DM1 at 0.2 mg/kg (toxin, equal to 22.57 mg/kg GQ1001), respectively. 5 animals/gender/group of the animals were necropsied on Day 7 while the others on Day 22. Toxicological parameters assessed included clinical observation, body weight, food consumption, clinical pathology (hematology, coagulation, and plasma chemistry), and pathology (gross pathology, organ weights, and histopathology).

Single-dose toxicity in cynomolgus monkeys

A GLP-compliant single-dose toxicology study was conducted in Cynomolgus monkeys. A total of 30 Cynomolgus monkeys (3 animals/gender/group) were given single intravenous infusion (20 min/dose/monkey) of vehicle (GQ1001 preparation buffer) at 0 mg/kg, or GQ1001 at 10, 30, and 45 mg/kg, or mAb at 45 mg/kg. Animals were necropsied after 6-week observation period on Day 43. The following parameters were evaluated: Clinical observation, body weight, food consumption, body (rectal) temperature, clinical pathology (hematology, coagulation, and plasma chemistry), and pathology (gross pathology and organ weights), as well as toxicokinetics and ADA evaluations.

Repeated-dose toxicity in cynomolgus monkeys

A GLP-compliant, pivotal, 7-week repeated-dose toxicology study was conducted in Cynomolgus monkeys. 40 cynomolgus monkeys (5/gender/group) were randomly assigned and were administered with GQ1001 (10, 30, and 45 mg/kg) or vehicle (0 mg/kg), once every 3 weeks for a total of 3 times in a 7-week dosing phase. At the end of the dosing phase, 3 animals/gender/group were necropsied, and the remaining 2 animals/gender/group were necropsied after a 6-week recovery phase. The following parameters were assessed: Clinical observations (including functional assessment of central nervous system), body weight, food consumption, ophthalmology, body temperature (rectal), local irritation, cardiovascular and respiratory system (ECG, body temperature (surface), and respiratory frequency) function, hematology, coagulation, plasma chemistry, urinalysis, immunophenotype, immunoglobulins, complements, gross pathology, organ weights, and microscopic histopathology, as well as concurrent toxicokinetics and ADA evaluations.

Statistics

Continuous data of repeated experiments (≥ 3 times) were shown as mean ± standard error (SE), and continuous data of different individuals were summarized as mean ± standard deviation (SD). Continuous data were compared between 2 groups using *t* or Wilcoxon test where appropriate, and across multiple groups using ANOVA or Kruskal-Wallis test followed by intergroup multiple comparisons where appropriate. IC_{50} and EC_{50} were determined using a 4-parameter logistic model[10]. A linear mixed-effects model was used to test the difference in the rate of tumor volume change over time among different groups[49]. Microsoft Office LTSC 2024 Preview was used for data collection. R 4.2.0 (https://www.r-project.org) was used for statistical analysis, and GraphPad Prism 9 for generating plots. Two-tailed $P < 0.05$ indicated statistical significance.

Ethics

This research complies with all relevant ethical regulations. This study and the protocol were approved by the local Institutional Review Boards of Fudan University Shanghai Cancer Center and The Fifth Medical Center of PLA General Hospital and the Institutional Animal Care and Use Committee (IACUC) of each contract research organization (Wuxi AppTec Co. Ltd. IACUCs (Nantong, Shanghai, and Suzhou), and the IACUCs of Lidebiotech (Shanghai and Xi'an), Genepharma, and Champions Oncology). The maximal tumor size permitted was 2500 mm^3, which was not exceeded. Sex was considered in the study design and analysis. Information on experimental animals is detailed in Supplementary Table 31. Animals had free access to sterilized dry granule food and sterile drinking water during the entire study period (temperature: 20–26 °C; humidity: 40–70%; 12-h light and 12-h dark cycle).

Reporting summary

Further information on research design is available in the Nature Portfolio Reporting Summary linked to this article.

Data availability

Source data are provided with this paper as the "Source Data.xlsx" file. Source data are provided with this paper.

References

1. Dumontet, C., Reichert, J. M., Senter, P. D., Lambert, J. M. & Beck, A. Antibody-drug conjugates come of age in oncology. *Nat. Rev. Drug Discov.* **22**, 641–661 (2023).
2. Beck, A., Goetsch, L., Dumontet, C. & Corvaïa, N. Strategies and challenges for the next generation of antibody-drug conjugates. *Nat. Rev. Drug Discov.* **16**, 315–337 (2017).
3. Habara, H. et al. Transition of average drug-to-antibody ratio of trastuzumab deruxtecan in systemic circulation in monkeys using a hybrid affinity capture liquid chromatography-tandem mass spectrometry. *Biopharmaceutics drug disposition* **44**, 380–384 (2023).
4. Anami, Y. et al. Homogeneity of antibody-drug conjugates critically impacts the therapeutic efficacy in brain tumors. *Cell Rep.* **39**, 110839 (2022).
5. Hamblett, K. J. et al. Effects of drug loading on the antitumor activity of a monoclonal antibody drug conjugate. *Clin. Cancer Res.: J. Am. Assoc. Cancer Res.* **10**, 7063–7070 (2004).
6. Conte, P. et al. Drug-induced interstitial lung disease during cancer therapies: expert opinion on diagnosis and treatment. *ESMO open* **7**, 100404 (2022).
7. Swain, S. M. et al. Multidisciplinary clinical guidance on trastuzumab deruxtecan (T-DXd)-related interstitial lung disease/pneumonitis-Focus on proactive monitoring, diagnosis, and management. *Cancer Treat. Rev.* **106**, 102378 (2022).
8. Kumagai, K. et al. Interstitial pneumonitis related to trastuzumab deruxtecan, a human epidermal growth factor receptor 2-targeting Ab-drug conjugate, in monkeys. *Cancer Sci.* **111**, 4636–4645 (2020).
9. Hinrichs, M. J. & Dixit, R. Antibody drug conjugates: nonclinical safety considerations. *AAPS J.* **17**, 1055–1064 (2015).
10. Ogitani, Y. et al. DS-8201a, A Novel HER2-Targeting ADC with a Novel DNA topoisomerase i inhibitor, demonstrates a promising antitumor efficacy with differentiation from T-DM1. *Clin. Cancer Res.: J. Am. Assoc. Cancer Res.* **22**, 5097–5108 (2016).
11. Krop, I. E. et al. Phase I study of trastuzumab-DM1, an HER2 antibody-drug conjugate, given every 3 weeks to patients with HER2-positive metastatic breast cancer. *J. Clin. Oncol.:. J. Am. Soc. Clin. Oncol.* **28**, 2698–2704 (2010).
12. Poon, K. A. et al. Preclinical safety profile of trastuzumab emtansine (T-DM1): mechanism of action of its cytotoxic component retained with improved tolerability. *Toxicol. Appl. Pharmacol.* **273**, 298–313 (2013).
13. Lyon, R. P. et al. Self-hydrolyzing maleimides improve the stability and pharmacological properties of antibody-drug conjugates. *Nat. Biotechnol.* **32**, 1059–1062 (2014).
14. Tumey, L. N. et al. Mild method for succinimide hydrolysis on ADCs: impact on ADC potency, stability, exposure, and efficacy. *Bioconjugate Chem.* **25**, 1871–1880 (2014).
15. Shen, B. Q. et al. Conjugation site modulates the in vivo stability and therapeutic activity of antibody-drug conjugates. *Nat. Biotechnol.* **30**, 184–189 (2012).
16. Drago, J. Z., Modi, S. & Chandarlapaty, S. Unlocking the potential of antibody-drug conjugates for cancer therapy. *Nat. Rev. Clin. Oncol.* **18**, 327–344 (2021).
17. Olson, D. et al. HER2-Selective and reversible tyrosine kinase inhibitor tucatinib potentiates the activity of T-DM1 in preclinical models of HER2-positive breast cancer. *Cancer Res Commun.* **3**, 1927–1939 (2023).
18. Li, B. T. et al. HER2-mediated internalization of cytotoxic agents in ERBB2 amplified or mutant lung cancers. *Cancer Discov.* **10**, 674–687 (2020).
19. Liu, J. et al. Elucidating molecular mechanisms and therapeutic synergy: irreversible HER2-TKI plus T-Dxd for enhanced anti-HER2 treatment of gastric cancer. *Gastric Cancer* **27**, 495–505 (2024).
20. Tian, H. et al. Dramatic response to pyrotinib and T-DM1 in HER2-negative metastatic breast cancer with 2 activating HER2 mutations. *Oncologist* **28**, e534–e541 (2023).
21. Saleh, K. et al. Mechanisms of action and resistance to anti-HER2 antibody-drug conjugates in breast cancer. *Cancer Drug Resist* **7**, 22 (2024).
22. Khoury, R. et al. Mechanisms of resistance to antibody-drug conjugates. *Int. J. Mol. Sci.* https://doi.org/10.3390/ijms24119674 (2023).
23. Guidi, L., Pellizzari, G., Tarantino, P., Valenza, C. & Curigliano, G. Resistance to antibody-drug conjugates targeting HER2 in breast cancer: molecular landscape and future challenges. *Cancers (Basel)* https://doi.org/10.3390/cancers15041130 (2023).
24. Gupta, A., Jatwani, K., Gupta, K., Qiu, J. & Dy, G. K. Loss of Rb1 associated with the onset of acquired resistance to trastuzumab deruxtecan in TP53-/HER2-mutated non-small-cell lung cancer: case series. *JCO Precis Oncol.* **7**, e2200476 (2023).
25. Díaz-Rodríguez, E., Gandullo-Sánchez, L., Ocaña, A. & Pandiella, A. Novel ADCs and strategies to overcome resistance to anti-HER2 ADCs. *Cancers (Basel)* https://doi.org/10.3390/cancers14010154 (2021).
26. Li, G. et al. Mechanisms of acquired resistance to trastuzumab emtansine in breast cancer cells. *Mol. Cancer Ther.* **17**, 1441–1453 (2018).
27. Weng, W. et al. Antibody-exatecan conjugates with a novel self-immolative moiety overcome resistance in colon and lung cancer. *Cancer Discov.* **13**, 950–973 (2023).
28. Nagai, Y., Oitate, M., Shiozawa, H. & Ando, O. Comprehensive preclinical pharmacokinetic evaluations of trastuzumab deruxtecan (DS-8201a), a HER2-targeting antibody-drug conjugate, in

cynomolgus monkeys. *Xenobiotica; fate foreign Compd. Biol. Syst.* **49**, 1086–1096 (2019).
29. Verma, S. et al. Trastuzumab emtansine for HER2-positive advanced breast cancer. *N. Engl. J. Med.* **367**, 1783–1791 (2012).
30. Byrne, A. T. et al. Interrogating open issues in cancer precision medicine with patient-derived xenografts. *Nat. Rev. Cancer* **17**, 254–268 (2017).
31. FDA, C. F. D. E. A. R. *APPLICATION NUMBER: 125427Orig1s000, PHARMACOLOGY REVIEW(S)*, https://www.accessdata.fda.gov/drugsatfda_docs/nda/2013/125427Orig1s000TOC.cfm (2013).
32. Guo, L. et al. Neratinib for HER2-positive breast cancer with an overlooked option. *Mol. Med. (Camb., Mass.)* **29**, 134 (2023).
33. Huang, L. et al. Decreasing resection rates for nonmetastatic gastric cancer in Europe and the United States. *Clin. Transl. Med.* **10**, e203 (2020).
34. Wei, Z. et al. LncRNA HOTAIR promotes the growth and metastasis of gastric cancer by sponging miR-1277-5p and upregulating COL5A1. *Gastric Cancer: J. Int. Gastric Cancer Assoc. Jpn. Gastric Cancer Assoc.* **23**, 1018–1032 (2020).
35. Modi, S. et al. Trastuzumab deruxtecan in previously treated HER2-low advanced breast cancer. *N. Engl. J. Med.* **387**, 9–20 (2022).
36. Li, B. T. et al. Trastuzumab deruxtecan in HER2-mutant non-small-cell lung cancer. *N. Engl. J. Med.* **386**, 241–251 (2022).
37. Lewis Phillips, G. D. et al. Targeting HER2-positive breast cancer with trastuzumab-DM1, an antibody-cytotoxic drug conjugate. *Cancer Res.* **68**, 9280–9290 (2008).
38. Thomas, A., Teicher, B. A. & Hassan, R. Antibody-drug conjugates for cancer therapy. *Lancet Oncol.* **17**, e254–e262 (2016).
39. Kovtun, Y. V. & Goldmacher, V. S. Cell killing by antibody-drug conjugates. *Cancer Lett.* **255**, 232–240 (2007).
40. Renault, K., Fredy, J. W., Renard, P. Y. & Sabot, C. Covalent Modification of Biomolecules through Maleimide-Based Labeling Strategies. *Bioconjug. Chem.* **29**, 2497–2513 (2018).
41. Integrated Genomic Characterization of Pancreatic Ductal Adenocarcinoma. *Cancer cell* **32**, 185-203, https://doi.org/10.1016/j.ccell.2017.07.007 (2017).
42. Burris, H. A. 3rd et al. Phase II study of the antibody drug conjugate trastuzumab-DM1 for the treatment of human epidermal growth factor receptor 2 (HER2)-positive breast cancer after prior HER2-directed therapy. *J. Clin. Oncol.:. J. Am. Soc. Clin. Oncol.* **29**, 398–405 (2011).
43. Shin, S. H. et al. An Elaborate New Linker System Significantly Enhances the Efficacy of an HER2-Antibody-Drug Conjugate against Refractory HER2-Positive Cancers. *Adv. Sci. (Weinh., Baden. -Wurtt., Ger.)* **8**, e2102414 (2021).
44. Huang, L. et al. Survival trends of patients with non-metastatic gastric adenocarcinoma in the US and European countries: the impact of decreasing resection rates. *Cancer Commun. (Lond., Engl.)* **42**, 648–662 (2022).
45. Huang, L. et al. Resection of pancreatic cancer in Europe and USA: an international large-scale study highlighting large variations. *Gut* **68**, 130–139 (2019).
46. Lu, G. et al. Co-administered antibody improves penetration of antibody-dye conjugate into human cancers with implications for antibody-drug conjugates. *Nat. Commun.* **11**, 5667 (2020).
47. Cilliers, C., Menezes, B., Nessler, I., Linderman, J. & Thurber, G. M. Improved tumor penetration and single-cell targeting of antibody-drug conjugates increases anticancer efficacy and host survival. *Cancer Res.* **78**, 758–768 (2018).
48. Colombo, R. & Rich, J. R. The therapeutic window of antibody drug conjugates: a dogma in need of revision. *Cancer cell* **40**, 1255–1263 (2022).
49. Sano, R. et al. An antibody-drug conjugate directed to the ALK receptor demonstrates efficacy in preclinical models of neuroblastoma. *Sci. Transl. Med.* https://doi.org/10.1126/scitranslmed.aau9732 (2019).

Acknowledgements

This study was supported by the National Science and Technology Major Project of the Ministry of Science and Technology of China (2019ZX09301165, G.Q.) by Development Center for Medical Science & Technology National Health Commission of the People's Republic of China, Suzhou Innovation and Entrepreneurship Leading Talents Project (ZXL2015056, G.Q.) by Suzhou Science and Technology Bureau, Jiangsu Foundation for Technology-based Start-up Incubation Program (BC2016021, G.Q.) by Jiangsu Provincial Department of Science and Technology, Jiangsu Municipal Natural Science Foundation for Youths (BK20160367, G.Q.) by Jiangsu Provincial Department of Science and Technology, National Natural Science Foundation of China (82203609, L.H.), and the Scientific Research Start-up Fund for Excellent Doctor (Youbo; Class A; L.H.) (The Third Batch) by The First Affiliated Hospital of Naval Medical University/Changhai Hospital, Naval Medical University. The funders had no role in study design; in the collection, analysis, or interpretation of data; in the writing of the report; or in the decision to submit the paper for publication. We are very grateful to Dr. Hong Que, Dr. Li Wan, and Dr. Meijun Xiong for their guidance and assistance during manuscript writing, and to Dr. Jing Ma for the guidance on the safety evaluation tests of GQ1001.

Author contributions

Conception and design: L.H., G.Q., C.G., Y. Sun, H.Y., C. Lv, C. Liu, L.J., J. Yuan, M.H., X.G., J. Yang, X.L., Y. Si, P.S., Y. Shi, L.S., B.Y. and B.W. Development of methodology: L.H., G.Q., C.G., Y. Sun, H.Y., C. Lv, C. Liu, L.J., J. Yuan, M.H., X.G., J. Yang, X.L., Y. Si, P.S., Y. Shi, L.S., B.Y. and B.W. Acquisition of data (provided animals, acquired and managed patients, provided facilities, etc.): L.H., G.Q., C.G., Y. Sun, H.Y., C. Lv, C. Liu, L.J., J. Yuan, M.H., X.G., J. Yang, X.L., Y. Si, P.S., Y. Shi, L.S., B.Y. and B.W. Analysis and interpretation of data (e.g., statistical analysis, biostatistics, computational analysis): L.H., G.Q., C.G., Y. Sun, H.Y., C. Lv, C. Liu, L.J., J. Yuan, M.H., X.G., J. Yang, X.L., Y. Si, P.S., Y. Shi, L.S., B.Y. and B.W. Writing of the manuscript: L.H. Review and/or revision of the manuscript: L.H., G.Q., C.G., Y. Sun, H.Y., C. Lv, C. Liu, L.J., J. Yuan, M.H., X.G., J. Yang, X.L., Y. Si, P.S., Y. Shi, L.S., B.Y. and B.W. Administrative, technical, or material support (i.e., reporting or organizing data, constructing databases): L.H., G.Q., C.G., Y. Sun, H.Y., C. Lv, C. Liu, L.J., J. Yuan, M.H., X.G., J. Yang, X.L., Y. Si, P.S., Y. Shi, L.S., B.Y. and B.W. Study supervision: G.Q., P.S., Y. Shi, L.S., B.Y. and B.W.

Competing interests

G.Q., Y. Sun, H.Y., C. Lv, C. Liu, J. Yuan, X.G., J. Yang, X.L., Y. Si, P.S., Y. Shi, and L.S. are shareholders in and/or employers/employees of GeneQuantum Healthcare Co., Ltd.; L.J. and M.H. are former GeneQuantum Healthcare employees. The remaining authors declare no competing interests.

Additional information

Supplementary information The online version contains supplementary material available at https://doi.org/10.1038/s41467-025-64675-6.

Correspondence and requests for materials should be addressed to Gang Qin, Paul Song, Yan Shi, Lili Shi, Bo Yang or Biyun Wang.

Peer review information *Nature Communications* thanks Nilay Sethi for their contribution to the peer review of this work. A peer review file is available.